Glycogen phosphorylase inhibition improves β-cell function

Journal:	*British Journal of Pharmacology*
Manuscript ID	2016-BJP-1084-RPT-G.R3
Manuscript Type:	Research Paper Themed Issue
Date Submitted by the Author:	n/a
Complete List of Authors:	Nagy, Lilla; Debreceni Egyetem, Department of Medical Chemistry; Magyar Tudomanyos Akademia, MTA-DE Cell Biology and Signaling Research Group Márton, Judit; Debreceni Egyetem, Department of Medical Chemistry Vida, András; Debreceni Egyetem, Department of Medical Chemistry; Magyar Tudomanyos Akademia, MTA-DE Lendület Laboratory of Cellular Metabolism Kiss, Gréta; Debreceni Egyetem, Department of Anatomy, Histology and Embryology Bokor, Éva; Debreceni Egyetem, Department of Organic Chemistry Sandor, Kun; Debreceni Egyetem, Department of Organic Chemistry Gönczi, Mónika; Debreceni Egyetem, Department of Physiology Docsa, Tibor; Debreceni Egyetem, Department of Medical Chemistry Tóth, Attila; University of Debrecen, Institute of Cardiology, Division of Clinical Physiology Antal, Miklós; Debreceni Egyetem, Department of Anatomy, Histology and Embryology; Magyar Tudomanyos Akademia, MTA-DE Neuroscience Research Group Gergely, Pál; Medical and Health Science Center, University of Debrecen, Department of Medical Chemistry Csóka, Balazs ; Rutgers New Jersey Medical School, Deptartment of Surgery ; Rutgers New Jersey Medical School, Center for Immunity and Inflammation Pacher, Pal; National institutes of Health, Somsák, László; Debreceni Egyetem, Department of Organic Chemistry Bai, Peter; Debreceni Egyetem, Department of Medical Chemistry; Debreceni Egyetem, Research Center for Molecular Medicine; Magyar Tudomanyos Akademia, MTA-DE Lendület Laboratory of Cellular Metabolism
Major area of pharmacology:	Endocrine pharmacology, Obesity/metabolic syndrome
Cross-cutting area:	Biochemical pharmacology, Diabetes
Additional area(s):	Metabolism, Post-translational modification, Repurposing

DEBRECENI EGYETEM
ÁLTALÁNOS ORVOSTUDOMÁNYI KAR
MOLEKULÁRIS MEDICINA KUTATÓKÖZPONT
Vezető: Dr. Fésüs László akadémikus

UNIVERSITY OF DEBRECEN
FACULTY OF MEDICINE
RESEARCH CENTRE FOR MOLECULAR MEDICINE
Head: László Fésüs M.D. Ph.D. MHASc

4032 Debrecen, Nagyerdei krt. 98., tel.: 36-52-255-478, fax: 36-52-255-539, e-mail: mmkk.office@med.unideb.hu
Levelezési cím: 4012 Debrecen, Pf. 67.

Dr Giuseppe Cirino PhD, FBPhS, FRBS
Editor of British Journal of Pharmacology

Debrecen, 3rd April 2017.

Dear Dr. Cirino,

Please find attached the revised version of our manuscript entitled „Glycogen phosphorylase inhibition improves β-cell function" to be reconsidered for scientific review in Your prestigious journal, British Journal of Pharmacology.

We have implemented the changes suggested by the Design & Analysis Editor and the Animal Ethics Editor into our manuscript and we provided detailed responses in a separate response letter.

We hope that the current form of the manuscript meets the high standards of Your Journal and would be very pleased if you would reconsider our paper for publication in British Journal of Pharmacology.

With best regards,

Peter Bai
Associate professor at the University of Debrecen

Glycogen phosphorylase inhibition improves β-cell function

Lilla Nagy[1,5], Judit Márton[1], András Vida[1,7], Gréta Kis[2], Éva Bokor[6], Sándor Kun[6], Mónika Gönczi[3], Tibor Docsa[1], Attila Tóth[4], Miklós Antal[2,12], Pál Gergely[1], Balázs Csóka[8,9], Pal Pacher[10], László Somsák[6], Péter Bai[1,7,11*]

Departments of [1]Medical Chemistry, [2] Anatomy, Histology and Embryology, [3]Physiology and [4]Cardiology, Faculty of Medicine, University of Debrecen, Debrecen, H-4032, Hungary

[5]MTA-DE Cell Biology and Signaling Research Group, Debrecen, H-4032, Hungary

[6]Department of Organic Chemistry, Faculty of Science and Technology, University of Debrecen, Debrecen, H-4032, Hungary

[7]MTA-DE Lendület Laboratory of Cellular Metabolism, Debrecen, H-4032, Hungary

[8]Department of Surgery and [9]Center for Immunity and Inflammation, Rutgers - New Jersey Medical School, Newark, NJ 07103, USA

[10]NIAAA, National Institutes of Health, Laboratory of Physiologic Studies, Rockville, MD 20852-1758, USA

[11]Research Center for Molecular Medicine, University of Debrecen, Debrecen, H-4032, Hungary

[12]MTA-DE Neuroscience Research Group, Debrecen, H-4032, Hungary

Running title: Glycogen phosphorylase inhibition in β-cells

*Whom correspondence should be sent to:

Peter Bai, PhD, DSc University of Debrecen, Department of Medical Chemistry, 4032 Debrecen, Egyetem tér 1., Hungary, Tel. +36 52 412 345; Fax. +36 52 412 566, e-mail: baip@med.unideb.hu

Abstract

Background and Purpose

Glycogen phosphorylase (GP) is the key enzyme for glycogen degradation. GP inhibitors (GPi-s) are glucose lowering agents trapping glucose in the liver as glycogen. Glycogen metabolism has implications in β-cell function; glycogen degradation can maintain cellular glucose levels, which feeds into catabolism to maintain insulin secretion, and elevated glycogen degradation levels contribute to glucotoxicity. The purpose of this study was to assess whether influencing glycogen metabolism in β-cells by GPi-s impacts β-cell function.

Experimental Approach

We used structurally different GPi-s in both MIN6 insulinoma cells and in mice.

Key Results

GPi treatment increased glycogen content and, consequently, the surface area of glycogen in MIN6 cells. Furthermore, GPi treatment induced insulin receptor β (IRβ), AKT, and p70S6K phosphorylation, as well as PDX1 and insulin expression. In line with these, GPi-s enhanced non-stimulated and glucose-stimulated insulin secretion in MIN6 cells. We showed that IRβ co-localizes with glycogen particles confirmed by an *in silico* screen, where components of IR signaling were identified as glycogen-bound proteins. GPi-s also induced the triggering pathway of insulin secretion marked by enhanced glycolysis, mitochondrial oxidation, and calcium signaling. Finally, GPi-s induced larger islets of Langerhans and improved glucose-induced insulin release in mice.

Conclusion and Implications

These data suggest that GPi-s also target β-cells and can be repurposed as agents to preserve β-cell function or even ameliorate β-cell dysfunction in different forms of diabetes.

Keywords: glycogen, glycogen phosphorylase, glycogen phosphorylase inhibitor, β-cell, PDX1, insulin, insulin synthesis, insulin receptor, insulin receptor signaling, mitochondria, PI3K

Abbreviations

AKT	Protein kinase B
BEVA335	3-ß-D-glucopyranosyl-5-(2-naphthyl)-1,2,4-triazole
CP-316819	5-Chloro-N-[(1S,2R)-2-hydroxy-3-(methoxymethylamino)-3-oxo-1-(phenylmethyl)propyl]-1H-indole-2-carboxamide
CTL	control
DPBS	Dulbecco's Phosphate Buffered Saline
ECAR	Extracellular Acidification Rate
EM	Electron microscopy
Fura-2AM	Fura-2 pentakis(acetoxymethyl) ester
GP	Glycogen phosphorylase
GPi-s	Glycogen phosphorylase inhibitors
GS	Glycogen synthase
GSIS	Glucose-stimulated insulin secretion
HFD	High fat diet
IR	Insulin receptor
IRβ	β subunit of insulin receptor
KB228	N-(3,5-dimethyl-benzoyl)-N'-(ß-D-glucopyranosyl)urea
KRBH	HEPES-balanced Krebs-Ringer phosphate buffer
mTORC1/2	Mammalian target of rapamycin complex 1 or 2
2NBDG	2-[N-(7-nitrobenz-2-oxa-1,3-diazol-4-yl) amino]-2-deoxy-D-glucose
OCR	Oxygen consumption rate
PAS	Periodic Acid Schiff
pCMV-βgal	β-galactosidase reporter gen with Cytomegalovirus promoter
PDK1	Phosphoinositide dependent protein kinase-1
PDX1	Pancreatic and duodenal homeobox 1
PI3K	Inositol-phosphate-3-kinase
RT	Room temperature
STF-1luc	Promoter of STF-1 homeodomain protein with luciferase reporter gene
WM	wortmannin

Introduction

Cellular glycogen content depends on the net of glycogen synthesis and degradation. Glycogen synthase (GS) is responsible for glycogen synthesis, while glycogen phosphorylase (GP) catalyzes glycogen breakdown to glucose. The two enzymes are regulated in an opposing fashion; only one of them is active at a time (Stalmans *et al.*, 1990). GP is a heterodimeric enzyme that possesses seven allosteric binding sites (Agius, 2015; Hayes *et al.*, 2014). The allosteric binding sites are potential targets for allosteric modulation by pharmacological agents. GP inhibitors, with a few exceptions, are not selective for the liver, muscle and brain isoforms of GP (Agius, 2007). Hence, current GP inhibitors likely block all GP activity in cells regardless of the proportions of GP isoforms. GP activation can significantly induce hepatic glucose production and modulate blood glucose levels. Consequently, GPi-s were tested as possible anti-diabetic agents to reduce blood glucose levels by storing glucose in the form of glycogen. GPi-s were tested in human clinical studies reaching phase II trials (Henke, 2012).

β-cells in the endocrine pancreas are responsible for the synthesis and secretion of insulin, a hormone that enables glucose uptake in tissues like skeletal muscle or white adipose. Insulin secretion is induced by glucose uptake, followed by glucose breakdown through glycolysis and mitochondrial oxidation leading to increases ATP levels. Increased production of ATP leads to the closing of ATP-sensitive potassium channels (K_{ATP}), and to increased calcium influx. Calcium influx induces the fusion of insulin-rich granules with the cell membrane leading to insulin secretion (MacDonald *et al.*, 2005). Since glucose is the major regulator of β-cell function, persistent hyperglycaemia combined with peripheral insulin resistance in type 2 diabetic conditions overworks β-cells to maintain normal blood glucose levels (Abdul-Ghani, 2013; Cerf, 2013; Halban *et al.*, 2014; MacDonald *et al.*, 2005). Chronic exposure to high glucose leads to the exhaustion of β-cells, progressive β-cell failure, and, eventually, to the loss of β-cells (Cerf, 2013).

Nevertheless, there are pathways that can counteract β-cell failure and loss. One such pathway is paracrine/autocrine insulin signaling through the insulin receptor (IR). IR signaling is a complex process that is initiated by the binding of insulin to its receptor, and leads to the autophosphorylation of the IR (Boucher *et al.*, 2014). IR autophosphorylation sets in motion a set of downstream phosphorylation events that involves the activation of phosphatidylinositol 3-kinase (PI3K) as well as the mechanistic target of rapamycin complex 1 and 2 (mTORC1 and 2). These master regulators induce the phosphorylation of protein

kinase B (AKT) and 70 kDa S6 kinase (p70S6K), and contribute to the stabilization and activation of pancreatic and duodenal homeobox 1 (PDX1) that is essential for β-cell survival and growth (Humphrey *et al.*, 2010; Johnson *et al.*, 2006; Kaneto *et al.*, 2015). These effects culminate in improved β-cell mass, survival, growth, and function (e.g. improved glucose-stimulated insulin secretion (GSIS) (Boucher *et al.*, 2014; Elghazi *et al.*, 2009; Fujimoto *et al.*, 2009; Rhodes *et al.*, 2013)).

Glycogen is abundant in pancreatic β-cells as compared to α, δ and pancreatic polypeptide-secreting cells, which contain glycogen only in negligible quantities (Graf *et al.*, 1984; Malaisse *et al.*, 2001). The abundance of glycogen in β-cells suggests a unique role for glycogen in these cells. However, the impact of intracellular glycogen content on β-cell function is still debatable (Graf *et al.*, 1981; Malaisse, 2016; Mir-Coll *et al.*, 2016). In the current study, we set out to investigate the effects of increased glycogen levels on β-cells.

Methods

Chemicals

Unless otherwise stated, all chemicals were purchased from *Sigma-Aldrich* (St. Louis, MO, USA) including CP-316819. Other GPi-s, namely KB228 and BEVA335, were synthesized in the laboratory of Dr. L. Somsák (**Fig.1A-C**). The inhibitors were used in concentrations close to their K_i to ensure pharmacological specificity: KB228 at 3 μM (K_i=937 nM) (Nagy *et al.*, 2013), BEVA335 at 1.5 μM (K_i=411 nM) (Bokor *et al.*, 2013) , and CP-316819 at 0.5 μM (K_i=220 nM). The K_i of CP-316819 was determined using the same methodology (Osz *et al.*, 1999) as for KB228 and Beva335 in order to gain comparable K_i values (**Fig.1D**).

Statement on the experimental approach

All animal and cell experiments were performed and analyzed by blinded researchers.

In all experiments animals were randomized between experimental cohorts. In cellular experiments the position of treatments on plates were randomly changed from experiment to experiment.

Animal studies

C57/Bl6J male mice (Charles River Laboratories, Wilmington, MA, USA) were used in the experiments as C57/Bl6J mice are good models for obesity-induced diabetes. Animal experiments were authorized by the Institutional Animal Care and Use Committee at the

University of Debrecen and the National Board for Animal Experimentation (7/2010 DE MÁB) and were carried out according to the NIH guideline "*Guide for the care and use of laboratory animals*", the ARRIVE guidelines and the applicable national laws.

We used C57/Bl6 male mice (6 months of age, 20-25 g). Experimentation took place at the Animal Facility of the University of Debrecen under SPF conditions. Mice were either kept on chow (10 kcal% of fat) (*SAFE*, *Augy, France*) or on high fat diet (HFD, hypercaloric diet, 60% fat content, *Research Diets, Inc., New Brunswick, NJ, USA*) for three months. Mice were either left untreated or treated with 90 mg kg^{-1} bodyweight of KB228 as a single intraperitoneal (i.p.) injection bolus once a week for ate least 3 weeks before sacrifice in PBS. Mice were sacrificed by cervical dislocation at the end of treatment. Tissues were collected and processed as specified. Mice were randomly incorporated into the vehicle or KB228 group. In the chow-fed cohorts there were 8 vehicle-treated and 8 KB228-treated mice, while in the HFD-fed cohorts there were 10 vehicle-treated and 10 KB228-treated mice. Altogether 36 mice were used in the study.

No more than six mice were housed in a cage (standard block shape 365x207x140 mm, surface 530 cm^2; 1284L Eurostandard Type II. L from Techniplast) with Lignocel Select Fine (*J. Rettenmaier und Söhne, Germany*) as bedding. Mice had paper tubes as environment enrichment. Dark/light cycle was 12 hours, 22±1 ^oC. Cages were changed once a week, on the same day. Mice had ad libitum access to food and water (sterilized tap water from the pipeline of the city). The animal facility is overseen by a veterinary. A total of 36 mice were used in the study, cohort sizes can be found in the figure captions.

Glucose-induced insulin release test

Glucose-induced insulin release test was performed as described in (Bai *et al.*, 2011). Briefly, mice were fasted overnight and the next morning ~50 µl blood was collected (baseline fasting insulin). After receiving 2 g kg^{-1} glucose by oral gavage, heparinized blood was collected from mice every 15 minutes up to 60 minutes. Heparinized plasma was prepared and plasma insulin content was measured using a commercial Mouse Insulin ELISA Kit (Mercodia, Uppsala, Sweden) following the manufacturer's instructions.

Histochemical assessment of glycogen content in pancreas

Glycogen content of pancreatic tissue was determined by Periodic Acid Schiff (PAS) staining. Deparaffinization was followed by hydration with water and oxidation of the 5 µm sections in 0.5% periodic acid solution for 20 minutes. After rinsing in distilled water,

sections were placed in Schiff reagent for 15 minutes. Sections were washed in lukewarm tap water for 5 minutes, then counterstained in hematoxylin for 2-3 minutes. After extensive washing with tap water, sections were dehydrated and covered. Microscopic images were acquired with a Zeiss Axioscope 20 microscope using Plan NEOFLUOR 40x objective at 25°C. Images were processed using Leica Application Suite V4.8 software. Glycogen content was determined by measuring the intensity with Image J software, where more intensive PAS staining correlates with higher glycogen content.

Insulin immunohistochemistry and islet size determination

Slides were deparaffinized, endogenous peroxidase activity was blocked (3% hydrogen peroxide in methanol on 5 μm paraffin sections for 15 minutes at RT), and then the slides were rinsed briefly with PBS. Non-specific binding was blocked by incubating the slides for 1 hour in 1% BSA diluted in PBS. To detect insulin, guinea pig polyclonal insulin antibody (DAKO, Glostrup, Denmark; 1:100) was applied overnight at 4 °C in 1% BSA diluted in PBS. After extensive washing with PBS, slides were stained with Envision one-step polymer HRP (BioGenex Fremont CA, USA) (90 minutes). Color reaction was developed for 2 minutes using nickel 3,3'-diaminobenzidine tetrachloride (Ni-DAB) as a substrate for antibody-coupled HRP (1.6 mM DAB, 140 mM NaCl, 90 mM $NiSO_4$, 100 mM Na-acetate, 3 mM H_2O_2, pH 6.6). After rinsing sections in 50 mM Tris-HCl (pH 7.4), the color was enhanced by incubating the sections for 2 minutes in 2% cobalt chloride (in 50 mM Tris-HCl, pH 7.2). Sections were then rinsed in distilled water and counterstained with 1% methyl green solution. A negative immunohistochemical control was included in each run. Microscopic images were acquired with a Zeiss Axioscope 20 microscope using Plan NEOFLUOR 40x objective at 25°C. Images were processed using Leica Application Suite V4.8 software. Islet size was determined in μm^2 by using Image J software.

Cell culture

MIN6 cells, a generous gift from Dr. J. Miyazaki (Osaka University Medical School, Japan) (Miyazaki *et al.*, 1990), were cultured in DMEM, 15% fetal calf serum, 1% L-glutamine, 1% penicillin-streptomycin, 50 μM 2-mercaptoethanol and 25 mM glucose. Treatments were performed at 5.5 mM glucose.

Biochemical glycogen determination

MIN6 cells were seeded at a concentration of $10x10^5$ per 10 cm^3 petri dish in 5.5 mM DMEM medium. One day after treatment, cells were removed by scraping and collected into Eppendorf tubes. The KOH-ethanol glycogen extraction method was used for extraction of glycogen and degradation to glucose. After the second ethanol wash, the supernatant was evaporated in a Speed-Vac and glycogen pellets were resuspended in distilled water, then phenol-sulfuric acid assay was applied. Three times volume of concentrated H_2SO_4 was added to each sample followed by 10 minutes of shaking at 500 rpm at RT. After adding 5% phenol solution to samples, we determined the cellular glycogen content spectrophotometrically. Absorbance was determined at 450 nm.

Electron microscopy (EM)

Pellets of cells after 1 day of GPi or vehicle treatment were processed for electron microscopic investigation according to the ferrocyanide-reduced osmium method described in (Karnovsky, 1971; Robinson *et al.*, 1982). Briefly, cells were fixed in 3% glutaraldehyde dissolved in 0.1 M cacodylate buffer (pH: 7.4) containing 5% sucrose for 1 hour at RT. After washing several times in cacodylate buffer (pH: 7.4), cells were post-fixed in ferrocyanide-reduced osmium (2% osmium tetroxide and 3% potassium ferrocyanide dissolved in 0.1 M cacodylate buffer, pH: 7.4) for 2 hours at RT. Following several washes in cacodylate buffer (pH: 7.4), cells were dehydrated and embedded into Durcupan ACM resin. Ultrathin sections were cut, collected on Formvar-coated single-slot grids, and counterstained with uranyl acetate and lead citrate. Sections were investigated with a JEOL 1010 transmission electron microscope and photographed at a magnification of 6000-10000x with an Olympus Veleta CCD camera. Digitalized images were processed with Adobe Photoshop CS5 software.

Morphometric assessment was accomplished as follows. The EM pictures of at least 10 different cells of each group were analyzed. The individual glycogen particles were counted, then their area and circumference (both in μm) were determined by using Image J software. Values were expressed as ratio between the total/individual circumference of the glycogen particles and the cross sectional area of the cell. To control the specificity of the staining, a group of cells underwent the same EM staining protocol without the addition of potassium ferrocyanide to osmium tetroxide (**Fig. 2E**).

Confocal microscopy

MIN6 cells were grown on glass coverslips for one day, then starved in glucose-free medium (XF Assay Medium Modified DMEM containing 0 mM glucose, 1% P/S, 1% L-glutamine, 10% FBS, Seahorse Bioscience) overnight. The cells were then charged with 500 µM fluorescent D-glucose analog (2-[N-(7-nitrobenz-2-oxa-1,3-diazol-4-yl) amino]-2-deoxy-D-glucose (2NBDG), Cayman Chemicals Company, Ann Arbor, Michigan, USA) in uptake buffer (pH 7.4, 138 mM NaCl, 5.5 mM D-glucose, 5 mM KCl, 1 mM $MgCl_2$, 1.5 mM $CaCl_2$, 10 mM Hepes) for 3 hours followed by incubation in 5.5 mM glucose-content medium for one day. Cells were then fixed with 100% methanol for 20 min at -20°C, then rinsed three times with 1x PBS. The cells were permeabilized with 1% Triton X-100 in PBS for 5 min, blocked with 1% BSA in PBS for 1 hour, and then incubated with primary monoclonal rabbit antibody (Insulin receptor β (IRβ, Cell signaling, 1:50) in a moist chamber overnight at 4°C followed by incubation with the secondary antibody (Alexa Fluor ® 647 donkey anti-rabbit IgG (H+L), Life Technologies, 1:1000) diluted in blocking solution for 1 hour at RT. Coverslips were rinsed three times with 1x PBS then cells were stained with DAPI special formation (NucBlue® Fixed cell Stain ReadyProbes™ reagent, Life Technologies, Carlesbad, Ca, USA) and rinsed in PBS again. Confocal images were acquired with a Leica TCS SP8 confocal microscope using HC PL APO CS2 63x/1.40 OIL immersion objective on a DMI6000 CS microscope at 25°C. The following lasers were used: OPSL 488 for 2NDBG, Diode 638 for Alexa Fluor 647, and 405 visible for DAPI. Images were processed using LAS X 2.0.1.14392 software. Nonspecific binding of the secondary antibodies was checked in control experiments.

Pdx1 promoter assay

Luciferase reporter assays were performed as in (Bai *et al.*, 2011). Cells were seeded at a concentration of $1.5x10^5$ MIN6 cells/well in 6-well plates, and were treated with GPi-s for 1 day. At the same time, cells were transfected with pCMV-βgal plasmid (1 µg) and -6500STF-1luc plasmid (Sharma *et al.*, 1996) (5 µg). Luciferase activity was measured using standard procedures, luciferase activity was expressed as luciferase activity/β-galactosidase activity, and the values were transformed to fold change compared to the control. The -6500STF-1luc plasmid was a generous gift from Dr. M. Montminy (Salk Institute, La Jolla, CA, USA). The promoter insert ($^{+}$68 - $^{-}$6500 bp) is of rat origin. To assess its applicability for murine models, we performed a sequence alignment of the promoter sequences and found 82% identity between the promoter sequence of rat and murine *Pdx1*. Upon densitometry

control samples were considered 1 and vales were expressed as fold change to reduce unwanted variation.

Gene expression and RT-qPCR

Reverse transcription coupled with real time quantitative PCR (RT-qPCR) reactions were performed similarly as in (Nagy *et al.*, 2013). Briefly, total RNA was prepared using TRIzol reagent (*Invitrogen*) according to the manufacturer's instructions. Two μg of RNA was used for reverse transcription (High Capacity cDNA Reverse Transcription Kit, Applied Biosystems, Foster City, CA, USA). The resulting cDNA, diluted 10X, was used for qPCR reactions (PCRBIOSYSTEMS, qPCRBIO SyGreen Mix Lo-ROX, United Kingdom). The qPCR reactions were performed using the Light-Cycler system (Roche Applied Science, Mannheim, Germany). Primers are listed in **Table 1**. Expression was normalized to the geometric mean of three control genes (cyclophillin, 18S, 36B4 or *Gapdh*). Control samples were considered 1 and values were expressed as fold change to reduce unwanted variation.

Table 1. Murine primers used in RT-qPCR reactions

Name	Forward	Reverse
18 S	5'-GGGAGCCTGAGAAACGGC-3'	5'-GGGTCGGGAGTGGGTAATTTT-3'
36B4	5'-AGATTCGGGATATGCTGTTGG-3'	5'-AAAGCCTGGAAGAAGGAGGTC-3'
Cyclophillin	5'-TGGAGAGCACCAAGACAGACA-3'	5'-TGCCGGAGTCGACAATGAT-3'
Gapdh	5'-CAAGGTCATCCATGACAACTTTG-3'	5'-GGCCATCCACAGTCTTCTGG-3'
Pdx1	5'-AATCCACCAAAGCTCACGCGTGGAA-3'	5'-TGATGTGTCTCTCGGTCAAGTTCAA-3'
Insulin	5'-GTGGGGAGCGTGGCTTCTTCTA-3'	5'-ACTGATCCACAATGCCACGCTTCT-3'

Protein extraction and western blotting

Cells were lysed in homogenization lysis buffer (250 mM saccharose, 20 mM Hepes, 1 mM EDTA, 1 mM EGTA, 0.5% Nonidet P-40). Cells were incubated on ice in lysis buffer then homogenized using a 26 G needle. Lysates were cleared by centrifugation. Supernatants contained the cytoplasmic fraction and the pellet contained the nuclear fraction. Pellets were further extracted first using "A" buffer (350 mM saccharose, 10 mM pH 7.9 Hepes, 3.3 mM $MgCl_2$, 10 mM KCl) then "B" buffer (the same as "A" excepting 250 mM saccharose). Sonicated samples were cleared by centrifugation. PDX1 was measured in the cytoplasmic and nuclear fractions; all others were measured in the cytoplasmic fractions. Western blotting experiments were performed as described in (Bai *et al.*, 2011). Blots were probed with the

antibodies listed in **Table 2**. Upon densitometry control samples were considered 1 and vales were expressed as fold change to reduce unwanted variation.

Table 2. List of antibodies used in the study

Primary antibodies:	**host**	**source**	**dilution**
Insulin (DAKO, Glostrup, Denmark)	guinea pig	polyclonal	1:1000
Insulin Receptor β (Cell signaling)	rabbit	monoclonal	1:1000
Phospho-Insulin Receptor β (Tyrosine 1345)(Cell signaling)	rabbit	monoclonal	1:500
PDX1 (Abcam) /cytoplasmic fraction/	rabbit	polyclonal	1:2000
PDX1 (Cell signaling) /nuclear fraction/	rabbit	monoclonal	1:1000
AKT (Sigma Aldrich)	rabbit	monoclonal	1:1000
Phospho-AKT (Serine 473) (Cell Signaling)	rabbit	monoclonal	1:2000
p70S6K (Cell Signaling)	rabbit	polyclonal	1:1000
Phospho-p70S6K (Threonine 389) (Cell Signaling)	rabbit	polyclonal	1:1000
LaminB1 (Cell signaling)	rabbit	monoclonal	1:1000
β-Actin−Peroxidase (Sigma Aldrich)	mouse	polyclonal	1:25000
Secondary antibodies:			
HRP-linked anti-rabbit IgG (Cell Signaling)	goat	polyclonal	1:2500
Peroxidase conjugated anti-guinea pig IgG (Sigma Aldrich)	goat	polyclonal	1:2000

Signals were developed using enhanced chemiluminescence (ECL) and were captured by Fluorchem FC2 gel documentation system (Alpha Innotech, San Leandro, CA, USA).

Insulin release in MIN6 cells

MIN6 cells were plated then pre-incubated in DMEM for 1 and 2 days with or without inhibitors. Before measurement, the medium was changed in each well to 1 ml of 5.5 mM glucose-content DMEM medium (without adding more glucose). After 2 minutes, a 10 µl sample was taken and diluted further in medium. Spontaneous and early insulin production by MIN6 cells was measured using a Mouse Insulin ELISA Kit (Mercodia, Winston Salem, N.C., USA) following the manufacturer's instructions. After the assay, 1 M NaOH was added

to adhered MIN6 cells in 6-well plates, and the total protein content was determined using BCA reagent (Pierce™ BCA Protein Assay Kit, Thermofisher, Walthman, MA, USA). Insulin secretion was normalized to protein content.

Glucose-induced insulin release in MIN6 cells

GSIS from MIN6 cells was determined using a static incubation protocol as in (Johnson *et al.*, 2007). MIN6 cells were cultured in 96-well plates until ~80% confluent, and the medium (25 mM glucose-contained) was changed every 48 h. On the day of the experiment, growth medium was removed, and the cells were washed twice with glucose-free KRBH (HEPES-balanced Krebs-Ringer phosphate buffer, composed of 111 mM NaCl, 25 mM $NaHCO_3$ (pH 7.4), 4.8 mM KCl, 1.2 mM KH_2PO_4, 1.2 mM $MgSO_4$, 10 mM HEPES, 2.3 mM $CaCl_2$ and 0.1% BSA). Cells were preincubated for 1 h in 5% CO_2 at 37°C in KRBH (1 mM glucose). The pre-incubation medium was removed, and the cells were washed once in glucose-free KRBH. The cells were then incubated for 1 h in 20 mM glucose-containing KRBH in the absence (control, CTL) or presence of inhibitors (KB228, BEVA335, CP-316819 and/or Wortmannin). At the same time, a set of control cells were incubated for 1 h in 1 mM glucose-containing KRBH for determination of insulin baseline. For all experiments, incubation medium was collected, spun at 1500 g for 5 min 4°C, and then diluted 20X. Insulin concentration in diluted samples was determined using a Mouse Insulin ELISA Kit (Mercodia, Winston Salem, N.C., USA). After the assay, 1 M NaOH was added to adhered MIN6 cells and the total protein content was determined using BCA reagent (Pierce™ BCA Protein Assay Kit, Thermofisher, Walthman, MA, USA). Insulin secretion was normalized to protein content.

Determination of total insulin protein in MIN6 cells

The same number of MIN6 cells were seeded in 24-well plate in 5.5 mM DMEM medium. After 1 day of treatment, cells were scraped and collected. Cells were extracted using 1.5% HCl in 70% ethanol overnight. After the extraction, insulin content in each sample was measured using a Mouse Insulin ELISA Kit (Mercodia, Winston Salem, N.C., USA) following the manufacturer's instructions. Insulin content was normalized for protein content then results were calculated as fold change with respect to the control.

Determination of oxygen consumption (OCR), and extracellular acidification rate (ECAR)

Oxygen consumption and extracellular acidification rates were determined using XF96 Flux Analyzer (Seahorse Biosciences, North Billerica, MA, USA). MIN6 cells were seeded in 96-well assay plates and treated with GPi-s for 1 and 2 days, followed by oximetry. After recording the baseline, OCR and ECAR were recorded every 3 minutes up to 60 minutes to follow the effects of GPi-s. Antimycin (10 μM) was used for distinguishing mitochondrial from non-mitochondrial oxygen consumption (proton leak). The final reading took place at 1 hour. OCR and ECAR were measured with respect to the cell number (10^5 cells) and readings were analyzed and plotted. The units were pmol O_2 x 10^5 MIN6 cells x $minute^{-1}$ for OCR and mpH x 10^5 MIN6 cells x $minute^{-1}$ for ECAR.

Measurement of changes in intracellular Ca^{2+} concentrations:

Calcium transients were assessed similarly as described in (Czikora *et al.*, 2012). MIN6 cells were seeded on glass coverslips (25 mm diameter and 1 mm thickness; Thermo Fisher (Thermo Fisher Scientific Gerhard Menzel B.V. & Co. KG, Braunschweig, Germany)) and treated with GPi-s for 1 or 2 days before calcium measurements. Cells were charged with 5 μM of Fura-2AM fluorescent Ca^{2+} indicator dye (Molecular Probes) for 90-120 minutes. Coverslips were then placed into a tissue chamber suitable for fluorescence microscopy. The tissue chamber was filled with DPBS (Invitrogen, containing calcium and magnesium) and was placed on the stage of an InCyte IM2 system (Intracellular Imaging Inc, Cincinnati, OH, USA). Cells were illuminated alternatively by 340 and 380 nm light (excitation) and pictures were recorded at a wavelength above 510 nm (emission). Six to eight obviously glucose responsive and clearly distinguishable cells for each treatment were selected in each regions of interest. Changes in intracellular Ca^{2+} concentration were recorded as changes in the ratio of the emission/excitation (340/380 nm). After reaching a stable baseline (min. 60 seconds), cells were induced with 20 mM glucose.

Determination of K_i

Kinetic measurements were performed as in (Osz *et al.*, 1999).

In silico screening for glycogen-binding proteins

The database containing a list of proteins with potential association with glycogen was assembled from multiple queries using the UniProt database (http://www.uniprot.org). The resulting list was manually revised and redundancies in the list were removed manually.

Statistical analysis

The data and statistical analysis comply with the recommendations on experimental design and analysis in pharmacology (Curtis *et al.*, 2015). All data are represented as average ± SEM, and n denotes the number of experiments. Statistical significance was determined using one-way ANNOVA with Tukey HSD. In the animal study to assess statistical significance unpaired, two-tailed Student's t test was used. Post-hoc tests were conducted only if the data in the experimental groups showed F distribution and no significant variance inhomogeneity. Technical replicates in a run were averaged that yielded a value for a biological replicate. The n number in the figure legends denote the number of biological replicates used for statistical analysis.

* indicates statistically significant differences between vehicle and treated groups at $p<0.05$.

Results

GP inhibition increases glycogen content and the size of glycogen particles in β-cells

In our study, we have used glucose analogue GPi-s (KB228 **(Fig. 1A)** (Nagy *et al.*, 2013) and BEVA335 (**Fig. 1B)** (Bokor *et al.*, 2013; Bokor *et al.*, 2015) that bring about mixed-type inhibition (Agius, 2007; Somsák *et al.*, 2008a). In addition, we have used a reference GPi (CP-316819 (**Fig. 1C**) (Rath *et al.*, 2000; Torres *et al.*, 2011)) which is an indole-2-carboxamide compound that binds to the novel allosteric site. To gain insight into the role of glycogen metabolism in β-cells, we used MIN6 cells, a well-established model for β-cells (Miyazaki *et al.*, 1990).

First, we assessed the presence of glycogen in MIN6 cells by incorporating a fluorescently labelled derivative of D-glucose (2NBDG) into glycogen followed by confocal microscopy. 2NBDG fluorescence appeared in MIN6 cells and displayed a punctate pattern in various sizes in the cytosol (**Fig. 2A**). Furthermore, when MIN6 cells were treated with GPi-s, cellular glycogen content was enhanced, as shown by the biochemical determination of glycogen (**Fig. 2B**), supporting an active glycogen metabolism in MIN6 cells. This observation was verified on EM sections of GPi-treated MIN6 cells stained for glycogen (**Fig. 2C**). Furthermore, image analysis enabled the measurement of the circumference of glycogen particles that we used as a proxy to glycogen particle surface. The circumference of glycogen particles also increased upon GPi treatment (**Fig. 2D, E**). Taken together, the application of GPi-s increases cellular glycogen content and the circumference of the glycogen particles suggesting a bigger glycogen particle surface area.

GP inhibition improves β-cell survival and β-cell function

In GPi-treated MIN6 cells, we observed elevated phosphorylation of IRβ on Tyrosine 1345 (**Fig. 3A**). Effectors lying downstream of IRβ, such as mTORC1 and mTORC2, were also activated, as evidenced by the enhanced phosphorylation of p70S6K protein on Threonine 389 and of AKT on Serine 473, respectively (**Fig. 3A**). Furthermore, we observed enhanced *Pdx1* promoter activity and mRNA expression upon GPi treatment that subsequently led to a large increase in PDX1 protein content both in the cytoplasmic and nuclear fraction (**Fig. 3B**). Insulin expression and protein levels were also increased upon GPi treatment (**Fig. 3C**). We have observed a tendency to increase in non-stimulated insulin release, while increases in GSIS were more pronounced upon GPi treatment (**Fig.3D, E**).

To explain these surprising data, we hypothesized that increases in glycogen content and glycogen particle size may provide additional surface area for binding and interaction with proteins involved in the regulation of β-cell function. We performed an *in silico* screen and identified more than 100 potential glycogen bound proteins (**Table 3**). Importantly, the list was dominated by members of the IR signaling pathway, and mTOR and AKT were found among the bound proteins. Furthermore, the GPi treatment-elicited phenotype shared features with IR activation (e.g. enhanced insulin production, activation of survival signals, such as AKT, etc. (Bernal-Mizrachi *et al.*, 2004)) suggesting that the binding of IR signaling proteins to glycogen is probably valid and functional.

Next, we tested whether the interaction that was detected *in silico* between glycogen particles and the IR exists in cells. First, we investigated the localization pattern of IRβ in MIN6 cells by immunofluorescence. IRβ displayed a punctate pattern (**Fig. 4A**), similarly to other reports of non-stimulated MIN6 cells (Shang *et al.*, 2009; Zhang *et al.*, 2001). We continued our investigations by performing co-localization studies using confocal microscopy. We opted for co-localization studies in intact cells by immunofluorescence due to the tenacious nature of glycogen. It is probable that in classical preparative biochemical assays, in which cells are lysed, glycogen is isolated, and the glycogen-bound proteins are analyzed, we may easily detect nonspecific proteins that bind to glycogen during preparation. Due to the lack of commercially available anti-glycogen antibody, we opted for charging glycogen with 2NBDG. Charging of cells with 2NBDG was not 100% efficient, we observed less fluorescently labelled glycogen particles than on EM pictures, making the evaluation of the fraction of glycogen-bound IRs impossible. The other suspected partner, IRβ, was stained with a specific antibody. When the two images were superimposed, a fraction of the IRβ and

glycogen particles co-localized (**Fig. 4B**). This observation coincided with GPi-induced phosphorylation of IRβ downstream targets. Taken together, GPi-s can induce IR signaling, probably through glycogen particles that interact with IRβ.

To reinforce the involvement of the insulin signaling pathway, we inhibited PI3K, a key participant in the IR cascade, with wortmannin (WM, 1 μM, 1 hour). Treatment of MIN6 cells with WM efficiently blocked the GPi-induced increases in mRNA and protein levels of PDX1 **(Fig. 5A)** and insulin **(Fig. 5B)**, as well as basal insulin release (**Fig. 5C**). However, GPi-induced GSIS was only slightly reduced by WM (**Fig. 5D**).

KB228 and CP316819 improves GSIS of β-cell

We next turned to investigate the effects of GP inhibition on the "classical" pathway of insulin release. Our first observation was that BEVA335 did not influence most features of the "classical" insulin secretion pathway; therefore, we omitted BEVA335 from further investigations and used only KB228 and CP-316819. Interestingly, the effects of KB228 and CP-316819 on the "classical" insulin release pathway lasted longer (2 days) than their effects on IR signaling (all experiments described in the previous sections were performed after 1 day of treatment).

CP-316819 enhanced glycolysis (as measured by ECAR) (**Fig. 6A**) and mitochondrial oxidation (as measured by OCR) (**Fig. 6B**). We have observed similar tendencies with KB228. Enhanced mitochondrial oxidation was translated into increases in glucose-stimulated calcium influx (**Fig. 6C**). These effects were discernible both at 1 day and 2 days of treatment; however, calcium uptake and the subsequent insulin release were more pronounced 2 days after treatment (**Fig. 6E**).

Repeated GPi treatment improves GSIS *in vivo*

We investigated the effects of repeated administration of KB228 in mice kept either on regular, low fat chow diet or HFD. PAS staining showed elevated pancreatic glycogen content upon KB228 treatment under both feeding regimens (**Fig. 7A**). In GPi-treated mice, we found a significant increase in Langerhans islet size in HFD-fed mice compared with vehicle-treated animals; Langerhans islet size also tended to be larger in chow-fed mice (**Fig. 7B**). Repeated administration of KB228 had a tendency to improve glucose-induced insulin release (**Fig. 7C**).

Discussion

In this study, we show that the pharmacological inhibition of GP and the consequent increase in cellular glycogen content was associated with induction of the insulin signaling pathway, β-cell proliferation, and glucose-induced insulin release. The role of glycogen in β-cells is controversial. Earlier studies (Malaisse *et al.*, 1993; Malaisse *et al.*, 1977) suggest that glycogenolysis provide glucose for glycolysis and mitochondrial oxidation in β-cells under starvation and, hence, facilitates insulin release. Under extremely high glucose concentrations, as in diabetes, glycogen accumulation in β-cells may lead to glucotoxicity (Malaisse, 2016; Malaisse *et al.*, 1992). However, a recent study by Mir-Coll provided contradictory results by showing that glycogen metabolism is not required for the maintenance of β-cell function. Furthermore, Mir-Coll (Mir-Coll *et al.*, 2016) showed that glycogen accumulation alone is not sufficient to trigger dysfunction, apoptosis and progression to diabetes in β-cells.

Our study supports those studies that show a physiological role for glycogen in β-cells (Doherty *et al.*, 2001; Graf *et al.*, 1981; Graf *et al.*, 1984; Hellman *et al.*, 1969; Malaisse, 2016; Malaisse *et al.*, 1993). We cannot provide a well-established explanation for the apparent discrepancy between these observations. Nevertheless, GPi-induced increases in glycogen is likely lower in our study than in others (Malaisse *et al.*, 1992) that may declutch different pathway. Similar differences in glycogen accumulation may account for the lack of glucotoxicity in our models (Malaisse *et al.*, 1992).

Prior studies have considered glycogen as a glucose reserve, while we suggest an additional structural role, according to which glycogen particles with elevated surface area contribute to the induction of IR signaling. Either glycogen itself induces IRβ autophosphorylation, or, more likely, glycogen serves as a scaffold for the members of the IR signaling pathway, as suggested by the *in silico* screen for glycogen-binding proteins. Other large cellular polymers (e.g. poly(ADP-ribose) (Bai, 2015; Tartier *et al.*, 2003)) or fuzzy proteins (Fuxreiter, 2012; Sharma *et al.*, 2015) were shown to act as interactive surfaces for large protein complexes in a similar fashion as we suggest here for glycogen.

GPi-induced biochemical changes involve several downstream targets of IR including PI3K, mTORC1, mTORC2, AKT and PDX1. The involvement of PI3K was evidenced by its blockade by WM which abolished GPi-induced increases in PDX1 and insulin expression, and non-stimulated insulin secretion. However, WM only modestly reduced GPi-mediated increases in GSIS, suggesting the involvement of other, yet unknown, pathway(s) also. The known biological functions of the other downstream GPi-induced factors fit well into the GPi-induced phenotype. The activation of PDX1 has been associated with improved transcription

and translation of insulin in β-cells (Kaneto *et al.*, 2015). Activation of mTORC1 and mTORC2 are prerequisites for cell growth and division (Sarbassov *et al.*, 2005), similar to PDX1 (Fujimoto *et al.*, 2009), while AKT is a survival signal in β-cells (Elghazi *et al.*, 2009).

Another route induced by GPi-s was the classical or triggering pathway of insulin secretion. Here, we show that KB228 and CP-316819 induces glycolysis, mitochondrial oxidation-and glucose-induced calcium transients —hallmarks of the classical pathway. In line with these observations, we also show a tendency towards improved GSIS in mice. Yet, we cannot explain how GPi-s induce the classical pathway. Nevertheless, GPi-s were reported to induce mitochondrial oxidation in previous reports (Baker *et al.*, 2006; Baker *et al.*, 2005; Nagy *et al.*, 2013). It would be an easy explanation that IR signaling can induce mitochondrial oxidation (Cheng *et al.*, 2010; Liu *et al.*, 2009) and this is what stands at the root of the phenotype. However, the activation of the insulin secretion cascade lasted longer (up to 2 days of treatment) than the induction of IR signaling (up to 1 day of treatment), suggesting additional mechanism(s).

GPi-s were originally designed to be used as glycogen lowering agents that trap excess glucose in the form of glycogen, mainly in the liver (Agius, 2007; Henke, 2012; Somsák *et al.*, 2008b). Several GPi-s were tested in clinical trials, passing phase I and confirming the safety of these drugs (Henke, 2012). Namely, CP-316819 (Pfizer, a drug used in our current study), AVE56588 (Sanofi-Aventis) and GSK1362885 (GlaxoSmithKline) completed phase I, while CP-368296 (Ingliforib, Pfizer) and PSN-357 (Prosidion, now Astellas Pharma) advanced to phase II (for review see (Henke, 2012)). The pro-proliferative effects of GPi-s in β-cells raise safety concerns if these were general and would affect a wide variety of cells. Nevertheless, Favaro et al. and Lee et al. (Favaro *et al.*, 2012; Lee *et al.*, 2004) showed that GPi-s are anti-proliferative in pancreatic adenocarcinoma cells suggesting a cell or tissue-specific proliferative effect. GPi clinical studies were halted after phase II; however, the reasons were not communicated (Henke, 2012). Our study suggests that that another cell type, β-cells, can be also targeted by GPi-s, and GPi-s exert beneficial effects in β-cells. Our data point out the positive effects of mild increases in glycogen in β-cells and demonstrate that GP inhibitors have the potential to act as β-cell preserving agents. These data raise the possibility of repurposing GP inhibitors from the original indication as agents to inhibit hepatic glucose output in type II diabetes to a new indication that is the preservation of β-cells in the context of type I or type II diabetes.

Conclusions

We show that structurally different GPi-s can induce synthesis and secretion of insulin and induce survival signals in a cellular model of β-cells. We propose that these effects of GPi-s are exerted through modulating insulin receptor signaling, where glycogen serves as a matrix clustering members of the signaling complex. In mice, the repeated administration of KB228, a GPi, led to the enlargement of the Langerhans islets and tended to increase glucose-induced insulin secretion. Taken together, we show a new target tissue for GPi-s and suggest repurposing these drugs to preserve β-cells function.

Author contributions

LN: planned and performed experiments, did the statistical analysis, and wrote the manuscript;

JM: performed RT-qPCR experiments;

AV: performed the in silico screening and did the statistical analysis;

GK: performed EM experiments;

ÉB and SK: synthesized GPi-s;

MG: performed ATP assay experiments;

TD: performed *in vivo* experiments;

AT: performed experiments and wrote the manuscript;

MA: planned and evaluated EM experiments;

PG: planned experiments and wrote the manuscript;

BC and PP: wrote the manuscript;

LS: designed and provided GPi-s and wrote the manuscript;

PB: planned, performed and evaluated experiments, and wrote the manuscript.

Acknowledgement

The authors acknowledge the critical revision of the manuscript by Dr. Karen L. Uray (Department of Medical Chemistry, University of Debrecen), the technical assistance of Mr. László Finta and the help of Attila Pap (Department of Biochemistry and Molecular Biology, University of Debrecen) for the help in describing the animal experiments.

Funding statement

Work by the authors was supported by the following:

Bolyai fellowship (MG); NKFIH (K108308, PD105808, K109450, K116940); GINOP-2.3.2-15-2016-00006 project that is co-financed by the European Union and the European Regional Development Fund; Momentum fellowship of the Hungarian Academy of Sciences and the University of Debrecen.

Conflict of interest statement

The authors declare no conflict of interest.

References

Abdul-Ghani MA (2013). Type 2 diabetes and the evolving paradigm in glucose regulation. *The American journal of managed care.* **19**(3 Suppl)**:** S43-50.

Agius L (2007). New hepatic targets for glycaemic control in diabetes. *Best Pract Res Clin Endocrinol Metab.* **21**(4)**:** 587-605.

Agius L (2015). Role of glycogen phosphorylase in liver glycogen metabolism. *Mol Aspects Med.* **46:** 34-45.

Bai P (2015). Biology of Poly(ADP-Ribose) Polymerases: The Factotums of Cell Maintenance. *Mol Cell.* **58**(6)**:** 947-958.

Bai P, Canto C, Brunyanszki A, Huber A, Szanto M, Cen Y*, et al.* (2011). PARP-2 Regulates SIRT1 Expression and Whole-Body Energy Expenditure. *Cell Metab.* **13**(4)**:** 450-460.

Baker DJ, Greenhaff PL, MacInnes A, Timmons JA (2006). The experimental type 2 diabetes therapy glycogen phosphorylase inhibition can impair aerobic muscle function during prolonged contraction. *Diabetes.* **55**(6)**:** 1855-1861.

Baker DJ, Timmons JA, Greenhaff PL (2005). Glycogen phosphorylase inhibition in type 2 diabetes therapy: a systematic evaluation of metabolic and functional effects in rat skeletal muscle. *Diabetes.* **54**(8)**:** 2453-2459.

Bernal-Mizrachi E, Fatrai S, Johnson JD, Ohsugi M, Otani K, Han Z*, et al.* (2004). Defective insulin secretion and increased susceptibility to experimental diabetes are induced by reduced Akt activity in pancreatic islet β cells. *Journal of Clinical Investigation.* **114**(7)**:** 928-936.

Bokor E, Docsa T, Gergely P, Somsak L (2013). C-Glucopyranosyl-1,2,4-triazoles As New Potent Inhibitors of Glycogen Phosphorylase. *ACS medicinal chemistry letters.* **4**(7)**:** 612-615.

Bokor E, Kun S, Docsa T, Gergely P, Somsák L (2015). 4(5)-Aryl-2-C-glucopyranosyl-imidazoles as New Nanomolar Glucose Analogue Inhibitors of Glycogen Phosphorylase. *ACS medicinal chemistry letters.* **6**(12)**:** 1215-1219.

Boucher J, Kleinridders A, Kahn CR (2014). Insulin Receptor Signaling in Normal and Insulin-Resistant States. *Cold Spring Harbor Perspectives in Biology.* **6**(1)**:** a009191.

Cerf ME (2013). Beta Cell Dysfunction and Insulin Resistance. *Frontiers in Endocrinology.* **4:** 37.

Cheng Z, Tseng Y, White MF (2010). Insulin signaling meets mitochondria in metabolism. *Trends Endocrinol Metab.* **21**(10)**:** 589-598.

Curtis MJ, Bond RA, Spina D, Ahluwalia A, Alexander SP, Giembycz MA*, et al.* (2015). Experimental design and analysis and their reporting: new guidance for publication in BJP. *Br J Pharmacol.* **172**(14)**:** 3461-3471.

Czikora A, Lizanecz E, Bako P, Rutkai I, Ruzsnavszky F, Magyar J*, et al.* (2012). Structure-activity relationships of vanilloid receptor agonists for arteriolar TRPV1. *Br J Pharmacol.* **165**(6)**:** 1801-1812.

Doherty M, Malaisse WJ (2001). Glycogen accumulation in rat pancreatic islets: in vitro experiments. *Endocrine.* **14**(3)**:** 303-309.

Elghazi L, Bernal-Mizrachi E (2009). Akt/PTEN: β-cell mass and pancreas plasticity. *Trends in endocrinology and metabolism: TEM.* **20**(5)**:** 243-251.

Favaro E, Bensaad K, Chong MG, Tennant DA, Ferguson DJ, Snell C*, et al.* (2012). Glucose Utilization via Glycogen Phosphorylase Sustains Proliferation and Prevents Premature Senescence in Cancer Cells. *Cell Metab.* **16**(6)**:** 751-764.

Fujimoto K, Polonsky KS (2009). Pdx1 and other factors that regulate pancreatic β-cell survival. *Diabetes, obesity & metabolism.* **11**(Suppl 4)**:** 30-37.

Fuxreiter M (2012). Fuzziness: linking regulation to protein dynamics. *Molecular bioSystems.* **8**(1)**:** 168-177.

Graf R, Klessen C (1981). Glycogen in pancreatic islets of steroid diabetic rats. Carbohydrate histochemical detection and localization using an immunocytochemical technique. *Histochemistry.* **73**(2)**:** 225-232.

Graf R, Tolken M (1984). Ultrastructural distribution of glycogen in pancreatic islets of steroid diabetic rats. *Basic and applied histochemistry.* **28**(4)**:** 391-397.

Halban PA, Polonsky KS, Bowden DW, Hawkins MA, Ling C, Mather KJ*, et al.* (2014). beta-cell failure in type 2 diabetes: postulated mechanisms and prospects for prevention and treatment. *Diabetes Care.* **37**(6)**:** 1751-1758.

Hayes JM, Kantsadi AL, Leonidas DD (2014). Natural products and their derivatives as inhibitors of glycogen phosphorylase: potential treatment for type 2 diabetes. *Phytochemistry Reviews.* **13**(2)**:** 471-498.

Hellman B, Idahl LA (1969). Presence and mobilization of glycogen in mammalian pancreatic beta cells. *Endocrinology.* **84**(1)**:** 1-8.

Henke BR (2012). Inhibition of Glycogen Phosphorylase as a Strategy for the Treatment of Type 2 Diabetes. In: Jones RM, Thurston DE, Rotella D (ed)^(eds). *New Therapeutic Strategies for Type 2 Diabetes: Small Molecule Approaches*, RSC drug discovery series edn: Royal Society of Chemistry. p^pp 324-365.

Humphrey RK, Yu SM, Flores LE, Jhala US (2010). Glucose regulates steady-state levels of PDX1 via the reciprocal actions of GSK3 and AKT kinases. *J Biol Chem.* **285**(5)**:** 3406-3416.

Johnson D, Shepherd RM, Gill D, Gorman T, Smith DM, Dunne MJ (2007). Glucose-dependent modulation of insulin secretion and intracellular calcium ions by GKA50, a glucokinase activator. *Diabetes.* **56**(6)**:** 1694-1702.

Johnson JD, Bernal-Mizrachi E, Alejandro EU, Han Z, Kalynyak TB, Li H*, et al.* (2006). Insulin protects islets from apoptosis via Pdx1 and specific changes in the human islet proteome. *Proceedings of the National Academy of Sciences of the United States of America.* **103**(51)**:** 19575-19580.

Kaneto H, Matsuoka T-a (2015). Role of Pancreatic Transcription Factors in Maintenance of Mature β-Cell Function. *International Journal of Molecular Sciences.* **16**(3)**:** 6281-6297.

Karnovsky M (1971). Use of ferrocyanide-reduced osmium tetroxide in electron microscopy. Abstr of 11 th Annual Meeting Am Soc Cell Biol: Rockefeller University Press, New York.

Lee WNP, Guo P, Lim S, Bassilian S, Lee ST, Boren J*, et al.* (2004). Metabolic sensitivity of pancreatic tumour cell apoptosis to glycogen phosphorylase inhibitor treatment. *British Journal of Cancer.* **91**(12)**:** 2094-2100.

Liu S, Okada T, Assmann A, Soto J, Liew CW, Bugger H*, et al.* (2009). Insulin signaling regulates mitochondrial function in pancreatic beta-cells. *PLoS One.* **4**(11)**:** e7983.

MacDonald PE, Joseph JW, Rorsman P (2005). Glucose-sensing mechanisms in pancreatic beta-cells. *Philos Trans R Soc Lond B Biol Sci.* **360**(1464)**:** 2211-2225.

Malaisse WJ (2016). Role of glycogen metabolism in pancreatic islet beta cell function. *Diabetologia.* **59**(11)**:** 2489-2491.

Malaisse WJ, Ladriere L, Cancelas J, Acitores A, Villanueva-Penacarrillo ML, Valverde I (2001). Pancreatic and hepatic glycogen content in normoglycemic and hyperglycemic rats. *Mol Cell Biochem.* **219**(1-2)**:** 45-49.

Malaisse WJ, Maggetto C, Leclercq-Meyer V, Sener A (1993). Interference of glycogenolysis with glycolysis in pancreatic islets from glucose-infused rats. *J Clin Invest.* **91**(2)**:** 432-436.

Malaisse WJ, Marynissen G, Sener A (1992). Possible role of glycogen accumulation in B-cell glucotoxicity. *Metabolism.* **41**(8)**:** 814-819.

Malaisse WJ, Sener A, Koser M, Ravazzola M, Malaisse-Lagae F (1977). The stimulus-secretion coupling of glucose-induced insulin release. Insulin release due to glycogenolysis in glucose-deprived islets. *Biochem J.* **164**(2)**:** 447-454.

Mir-Coll J, Duran J, Slebe F, Garcia-Rocha M, Gomis R, Gasa R*, et al.* (2016). Genetic models rule out a major role of beta cell glycogen in the control of glucose homeostasis. *Diabetologia.* **59**(5)**:** 1012-1020.

Miyazaki J, Araki K, Yamato E, Ikegami H, Asano T, Shibasaki Y*, et al.* (1990). Establishment of a pancreatic beta cell line that retains glucose-inducible insulin secretion: special reference to expression of glucose transporter isoforms. *Endocrinology.* **127**(1)**:** 126-132.

Nagy L, Docsa T, Szántó M, Brunyánszki A, Hegedűs C, Márton J*, et al.* (2013). Glycogen phosphorylase inhibitor N-(3,5-dimethyl-benzoyl)-N'-(β-D-glucopyranosyl)urea improves glucose tolerance under normoglycemic and diabetic conditions and rearranges hepatic metabolism. *PLoS One.* **8**(7)**:** e0069420.

Osz E, Somsak L, Szilagyi L, Kovacs L, Docsa T, Toth B*, et al.* (1999). Efficient inhibition of muscle and liver glycogen phosphorylases by a new glucopyranosylidene-spiro-thiohydantoin. *Bioorg Med Chem Lett.* **9**(10)**:** 1385-1390.

Rath VL, Ammirati M, Danley DE, Ekstrom JL, Gibbs EM, Hynes TR*, et al.* (2000). Human liver glycogen phosphorylase inhibitors bind at a new allosteric site. *Chemistry & biology.* **7**(9)**:** 677-682.

Rhodes CJ, White MF, Leahy JL, Kahn SE (2013). Direct autocrine action of insulin on beta-cells: does it make physiological sense? *Diabetes.* **62**(7)**:** 2157-2163.

Robinson JM, Karnovsky ML, Karnovsky MJ (1982). Glycogen accumulation in polymorphonuclear leukocytes, and other intracellular alterations that occur during inflammation. *The Journal of cell biology.* **95**(3)**:** 933-942.

Sarbassov DD, Ali SM, Sabatini DM (2005). Growing roles for the mTOR pathway. *Curr Opin Cell Biol.* **17**(6)**:** 596-603.

Shang Y, Liu Y, Du L, Wang Y, Cheng X, Xiao W*, et al.* (2009). Targeted expression of uncoupling protein 2 to mouse liver increases the susceptibility to lipopolysaccharide/galactosamine-induced acute liver injury. *Hepatology.* **50**(4)**:** 1204-1216.

Sharma R, Raduly Z, Miskei M, Fuxreiter M (2015). Fuzzy complexes: Specific binding without complete folding. *FEBS Lett.* **589**(19 Pt A)**:** 2533-2542.

Sharma S, Leonard J, Lee S, Chapman HD, Leiter EH, Montminy MR (1996). Pancreatic islet expression of the homeobox factor STF-1 relies on an E-box motif that binds USF. *J Biol Chem.* **271**(4)**:** 2294-2299.

Somsák L, Czifrák K, Tóth M, Bokor É, Chrysina ED, Alexacou KM*, et al.* (2008b). New inhibitors of glycogen phosphorylase as potential antidiabetic agents. *Current Medicinal Chemistry.* **15**(28)**:** 2933-2983.

Somsák L, Felföldi N, Kónya B, Hüse C, Telepó K, Bokor E*, et al.* (2008a). Assessment of synthetic methods for the preparation of N-β-d-glucopyranosyl-N′-substituted ureas, -thioureas and related compounds. *Carbohydrate Research.* **343**(12)**:** 2083-2093.

Stalmans W, Bollen M, Toth B, Gergely P (1990). Short-term hormonal control of protein phosphatases involved in hepatic glycogen metabolism. *Adv Enzyme Regul.* **30:** 305-327.

Tartier L, Spenlehauer C, Newman HC, Folkard M, Prise KM, Michael BD*, et al.* (2003). Local DNA damage by proton microbeam irradiation induces poly(ADP-ribose) synthesis in mammalian cells. *Mutagenesis.* **18**(5)**:** 411-416.

Torres TP, Sasaki N, Donahue EP, Lacy B, Printz RL, Cherrington AD*, et al.* (2011). Impact of a Glycogen Phosphorylase Inhibitor and Metformin on Basal and Glucagon-Stimulated Hepatic Glucose Flux in Conscious Dogs. *The Journal of Pharmacology and Experimental Therapeutics.* **337**(3)**:** 610-620.

Zhang CY, Baffy G, Perret P, Krauss S, Peroni O, Grujic D*, et al.* (2001). Uncoupling protein-2 negatively regulates insulin secretion and is a major link between obesity, beta cell dysfunction, and type 2 diabetes. *Cell.* **105**(6)**:** 745-755.

Figure legends

Figure 1. Structures of GP inhibitors

(A) KB228: N-(3,5-dimethyl-benzoyl)-N'-(ß-D-glucopyranosyl)urea, 3 µM final concentration (Ki=937 nM).

(B) BEVA335: 3-ß-D-glucopyranosyl-5-(2-naphthyl)-1,2,4-triazole, 1.5 µM final concentration (Ki=411 nM).

(C) CP-316819: 5-Chloro-N-[(1S, 2R)-2-hydroxy-3-(methoxymethylamino)-3-oxo-1-(phenylmethyl) propyl]-1H-indole-2-carboxamide, 0.5 µM final concentration (K_i=209 nM).

(D) Kinetics inhibition of glycogen phosphorylase b by CP316819 were analysed at constant concentration of glycogen (1 m/V%), and varying concentrations of glucose-1-phosphate (4-40 mM). Replotting the slopes of double reciprocal plots against the effective inhibitor concentrations the secondary plot where analysed, which show the Ki for the inhibitor.

Figure 2. The effects of GPi-s on glycogen content and on the size of glycogen particles in β-cells

(A) In MIN6 cells, the cytosolic localization of glycogen granules was analyzed in confocal microscopy experiments. After incorporation of fluorescent labelled derivative of D-glucose (2NBDG, green) into glycogen the nuclei were visualized by staining with DAPI (in blue). White arrows point to representative glycogen particles. Bars represent 5 µm. Brightness and contrast was adjusted on that panel.

(B) MIN6 cells were treated with GP inhibitors at the concentrations indicated for 24 hours, then glycogen content was determined in phenol-sulfuric colorimetric assays (n=6, in duplicate).

(C-D) Alternatively, glycogen was assessed by morphometric analysis of ultrasections of ferrocyanide-reduced osmium-stained MIN6 cells. (C) Quantification of glycogen content in cells (n=5, 10 cells analyzed per run) and (D) the circumference of the total glycogen particle in cells (n=5, 10 cells analyzed per run) were determined on EM sections.

(E) Representative EM sections are presented. Red arrows point to representative glycogen granules (bars = 2 µm).

Figure 3. GP inhibitors induce insulin receptor signaling in MIN6 cells

MIN6 cells were treated with GPi-s for 1 day at the indicated concentrations. In these cells **(A)** phosphorylation of IRβ subunit on Tyrosine 1345, AKT on Serine 473 and S6K on Threonine 389 were assessed by Western blot analysis of phosphorylated and non-phosphorylated forms of the respective proteins. One representative blot is presented. **(B)** *Pdx1* promoter activity (n=5, in duplicate) by luciferase assay and mRNA levels (n=5, in duplicate or triplicate) by RT-qPCR were determined. PDX1 protein levels were determined in the cytoplasmic and nuclear fractions of MIN6 cell lysates by Western blotting. One representative blot is presented here. **(C)** In GPi-treated cells, insulin mRNA expression (n=5, in duplicate or triplicate), the corresponding protein levels (n=5) as well as **(D)** insulin release (n=6) were determined. **(E)** GSIS were analyzed by insulin ELISA Kit (n=5).

Figure 4. Co-localization of glycogen particles and β subunit of insulin receptor in MIN6 cells.

(A) Localization of IRβ and its **(B)** co-localization with glycogen in MIN6 cells were assessed in confocal microscopy experiments (n=8). Glycogen was charged with a fluorescent glucose analog (2NBDG, green), IRβ was immunostained using an IRβ-specific antibody and Alexa Fluor 647 secondary antibody (red). Nuclei of the cells were stained using DAPI (blue). Bars represent 5 μm, on the inlay of panel A the bar represents 3.5 μm. IRβ staining was completely lost when the primary antibody was omitted during immunostaining. On the inlay of panel A brightness and contrast was adjusted.

Figure 5. Inhibition of PI3K by WM abolished the effects of GPi-s in MIN6 cells.

MIN6 cells were treated with GPi-s as before and a subset of MIN6 cells were treated with wortmannin (WM, 1 μM, for the last hour of the GPi treatment). In these cells mRNA (n=5, in duplicate) and protein levels (n=5, in duplicate) of **(A)** PDX1 and **(B)** insulin were determined. For determination of insulin, total protein was extracted and insulin was quantified by Mouse Insulin ELISA Kit. Finally, **(C)** non-stimulated, spontaneous (n=5) and **(D)** glucose-induced (n=5) insulin secretion were assessed.

Figure 6. GP inhibitor KB228 and CP-316819 induce the "classical" insulin secretion pathway in MIN6 cells.

MIN6 cells were treated with GPi-s for 1 and 2 days. In these cells **(A)** extracellular acidification rate (ECAR) and **(B)** cellular oxygen consumption rate (OCR) (n=7, in quadruplicate or octuplicate) were determined by Seahorse extracellular flux analyzer. **(C)**

Calcium influx was induced by 20 mM glucose and was determined by fura-2AM staining (n=5, 6-8 area of interest). Furthermore, GSIS **(D)** (n=5) was determined by Mouse Insulin ELISA Kit. Insulin baseline was measured at 1 mM glucose concentration, while glucose stimulation was performed with 20 mM glucose similarly to the measurement of Ca^{2+}-oscillation.

Figure 7. In vivo effects of KB228 treatment

Chow- and HFD-fed C57/Bl6J male mice underwent repeated vehicle or KB228 treatment (weekly, 90 mg kg^{-1} i.p) for at least three consecutive weeks. After sacrifice **(A)** glycogen content was evaluated on PAS-stained slides. Representative images are presented (scale bar = 50 μm). PAS positivity was evaluated by measuring the intensity of staining with Image J software. **(B)** The size of islets of Langerhans were determined on insulin-immunostained histological sections (scale bars = 50 μm). Representative images are shown. Islet size was determined in μm^2 by using Image J software. We used Student's t-test (unpaired, two-tailed) for statistical analysis. **(C)** Glucose-induced increases in serum insulin was determined using insulin-specific ELISA kit.

Table 3. List of the glycogen binding proteins

PATHWAY/CATEGORY	GENE	PROTEIN NAME(S)
GLYCOGEN METABOLISM	SLC2A2	Solute carrier family 2, facilitated glucose transporter member 2 (Glucose transporter type 2, liver) (GLUT-2)
	GYG2	Glycogenin-2 (GN-2) (GN2) (EC 2.4.1.186)
	GYG1	Glycogenin-1 (GN-1) (GN1) (EC 2.4.1.186)
	TRIM7	Tripartite motif-containing protein 7 (Glycogenin-interacting protein) (RING finger protein 90)
	UGP1	UTP--glucose-1-phosphate uridylyltransferase (EC 2.7.7.9)
	GYS1	Glycogen [starch] synthase, muscle (EC 2.4.1.11)
	GYS2	Glycogen [starch] synthase, liver (EC 2.4.1.11)
	GBE1	1,4-alpha-glucan-branching enzyme (EC 2.4.1.18) (Brancher enzyme)
	PYGL	Alpha-1,4 glucan phosphorylase (EC 2.4.1.1)
	PYGB	Alpha-1,4 glucan phosphorylase (EC 2.4.1.1) (Fragment)
	PYGM	Glycogen phosphorylase, muscle form (EC 2.4.1.1) (Myophosphorylase)
	SI	Sucrase-isomaltase, intestinal [Cleaved into: Sucrase (EC 3.2.1.48)
	GAA	Lysosomal alpha-glucosidase (EC 3.2.1.20)
	AGL	Glycogen debranching enzyme (Glycogen debrancher)
	PHKA1	Phosphorylase b kinase regulatory subunit alpha, skeletal muscle isoform (Phosphorylase kinase alpha M subunit)
	PHKA2	Phosphorylase b kinase regulatory subunit alpha, liver isoform (Phosphorylase kinase alpha L subunit)
	PHKB	Phosphorylase b kinase regulatory subunit beta (Phosphorylase kinase subunit beta)
	PHKG1	Phosphorylase b kinase gamma catalytic chain, skeletal muscle/heart isoform
	PHKG2	Phosphorylase b kinase gamma catalytic chain, liver/testis isoform (PHK-gamma-LT) (PHK-gamma-T) (EC 2.7.11.19)
INSULIN RECEPTOR SIGNALING	INSR	Insulin receptor (IR) (EC 2.7.10.1)
	INS	Insulin
	IAPP	Islet amyloid polypeptide (Amylin) (Diabetes-associated peptide) (DAP) (Insulinoma amyloid peptide)
	IRS1	Insulin receptor substrate 1 (IRS-1)
	IRS2	Insulin receptor substrate 2 (IRS-2)
	PIK3R1	Phosphatidylinositol 3-kinase regulatory subunit alpha (PI3-kinase regulatory subunit alpha)

	INPP5K	Inositol polyphosphate 5-phosphatase K (EC 3.1.3.56)
	GSK3A	Glycogen synthase kinase-3 alpha (GSK-3 alpha) (EC 2.7.11.26)
	GSK3B	Glycogen synthase kinase-3 beta (GSK-3 beta) (EC 2.7.11.26)
	NIN	Ninein (hNinein) (Glycogen synthase kinase 3 beta-interacting protein) (GSK3B-interacting protein)
	AKT2	Protein kinase B beta (EC 2.7.11.1)
	GRB10	Growth factor receptor-bound protein 10 (GRB10 adapter protein) (Insulin receptor-binding protein Grb-IR)
	IGF1	Insulin-like growth factor I (IGF-I) (Mechano growth factor) (MGF) (Somatomedin-C)
	IGF2	Insulin-like growth factor II (IGF-II) (Somatomedin-A)
mTOR AND AMPK	MTOR	Serine/threonine-protein kinase mTOR (EC 2.7.11.1)
	RPS6KA3	Ribosomal protein S6 kinase alpha-3 (S6K-alpha-3) (EC 2.7.11.1)
	PRKAB1	5'-AMP-activated protein kinase subunit beta-1 (AMPK subunit beta-1) (AMPKb)
	PRKAG2	5'-AMP-activated protein kinase subunit gamma-2 (AMPK gamma2) (AMPK subunit gamma-2) (H91620p)
	PRKAG3	5'-AMP-activated protein kinase subunit gamma-3 (AMPK gamma3) (AMPK subunit gamma-3)
HORMONES, HORMONAL SIGNALING	PTH	Parathyroid hormone (PTH) (Parathormone) (Parathyrin)
	ADIPOQ	Adiponectin
	POMC	Pro-opiomelanocortin (POMC)
	GCGR	Glucagon receptor (GL-R)
	ADRA1B	Alpha-1B adrenergic receptor (Alpha-1B adrenoreceptor) (Alpha-1B adrenoceptor)
INFLAMMATORY	NFATC1	Nuclear factor of activated T-cells, cytoplasmic 1 (NF-ATc1)
	NFKB1	Nuclear factor NF-kappa-B p105 subunit (DNA-binding factor KBF1)
	GLI3	Transcriptional activator GLI3 (GLI3 form of 190 kDa)
	IL6ST	Interleukin-6 receptor subunit beta
	RELA	Transcription factor p65 (Nuclear factor NF-kappa-B p65 subunit)
OTHER SIGNALING	CALM1	Calmodulin (CaM)
	DUSP13	Dual specificity protein phosphatase 13 isoform A (DUSP13A) (EC 3.1.3.16)

	DYRK1A	Dual specificity tyrosine-phosphorylation-regulated kinase 1A (EC 2.7.12.1)
	DYRK1B	Dual specificity tyrosine-phosphorylation-regulated kinase 1B (EC 2.7.12.1) (Minibrain-related kinase) (Mirk protein kinase)
	DYRK2	Dual specificity tyrosine-phosphorylation-regulated kinase 2 (EC 2.7.12.1)
	PTPRE	Receptor-type tyrosine-protein phosphatase epsilon (EC 3.1.3.48)
	PRUNE	Protein prune homolog (hPrune) (EC 3.6.1.1)
	SGK3	Serine/threonine-protein kinase Sgk3 (EC 2.7.11.1)
	SORBS1	Sorbin and SH3 domain-containing protein 1 (Ponsin) (SH3P12) (c-Cbl-associated protein) (CAP)
	STK40	SINK-homologous serine/threonine-protein kinase (Sugen kinase 495) (SgK495)
	TBK1	Serine/threonine-protein kinase TBK1 (EC 2.7.11.1)
	PPP1CA	Serine/threonine-protein phosphatase PP1-alpha catalytic subunit (PP-1A) (EC 3.1.3.16)
	PPP1R2P1	Putative protein phosphatase inhibitor 2-like protein 1 (Protein phosphatase 1, regulatory subunit 2 pseudogene 1)
	PPP1R2P3	Protein phosphatase inhibitor 2-like protein 3 (Protein phosphatase 1, regulatory subunit 2 pseudogene 3)
	PPP1R2 IPP2	Protein phosphatase inhibitor 2 (IPP-2)
	AKT1	Protein kinase B (PKB) (Protein kinase B alpha) (PKB alpha)
	PASK	PAS domain-containing serine/threonine-protein kinase (PAS-kinase) (PASKIN) (hPASK) (EC 2.7.11.1)
	AXIN1	Axin-1 (Axis inhibition protein 1) (hAxin)
	AXIN2	Axin-2 (Axin-like protein) (Axil) (Axis inhibition protein 2) (Conductin)
	PER2	Period circadian protein homolog 2 (hPER2) (Circadian clock protein PERIOD 2)

OTHER CARBOHYDRATE METABOLISM	GCK	Glucokinase (EC 2.7.1.2)
	PFKM	ATP-dependent 6-phosphofructokinase, muscle type (ATP-PFK) (PFK-M) (EC 2.7.1.11)
	PGM1	Phosphoglucomutase-1 (PGM 1) (EC 5.4.2.2)
	PGM2	Phosphoglucomutase-2 (PGM 2) (EC 5.4.2.2)
	PGAM2	Phosphoglycerate mutase 2 (EC 3.1.3.13)
	PGK1	Phosphoglycerate kinase 1 (EC 2.7.2.3)
	ALDOA	Fructose-bisphosphate aldolase A (EC 4.1.2.13)
	LDHA	L-lactate dehydrogenase A chain (LDH-A) (EC 1.1.1.27)

	LDHB	L-lactate dehydrogenase B chain (LDH-B) (EC 1.1.1.27)
	ENO3	Beta-enolase (EC 4.2.1.11)
	KHK	Ketohexokinase (EC 2.7.1.3) (Hepatic fructokinase)
	G6PC3	Glucose-6-phosphatase 3 (G-6-Pase 3) (G6Pase 3) (EC 3.1.3.9)
	FBP2	Fructose-1,6-bisphosphatase isozyme 2 (FBPase 2) (EC 3.1.3.11)
	HNF1A	Hepatocyte nuclear factor 1-alpha (HNF-1-alpha) (HNF-1A)
	SLC37A4	Glucose-6-phosphate translocase (Glucose-5-phosphate transporter)
LIPID METABOLISM	APOA5	Apolipoprotein A-V (Apo-AV)
	THEM4	Acyl-coenzyme A thioesterase THEM4 (Acyl-CoA thioesterase THEM4) (EC 3.1.2.2)
	ACADM	Medium-chain specific acyl-CoA dehydrogenase, mitochondrial (MCAD) (EC 1.3.8.7)
	FASN	Fatty acid synthase (EC 2.3.1.85)
	PTGES3	Prostaglandin E synthase 3 (EC 5.3.99.3)
UREA CYCLE	CPS1	Carbamoyl-phosphate synthase [ammonia], mitochondrial (EC 6.3.4.16) (Carbamoyl-phosphate synthetase I) (CPSase I)
TRANSCRIPTION AND TRANSLATION	TCF7L2	Transcription factor 7-like 2 (HMG box transcription factor 4) (T-cell-specific transcription factor 4) (T-cell factor 4) (TCF-4) (hTCF-4)
	NR1D1	Nuclear receptor subfamily 1 group D member 1 (Rev-erbA-alpha) (V-erbA-related protein 1) (EAR-1)
	EIF2B5	Translation initiation factor eIF-2B subunit epsilon (eIF-2B GDP-GTP exchange factor subunit epsilon)
	TCF7L2	TCF7L2 protein (Transcription factor 7-like 2 (T-cell specific, HMG-box), isoform CRA_e)
PROTEIN DEGRADATION	BTRC	F-box/WD repeat-containing protein 1A (E3RSIkappaB)
	NHLRC1	E3 ubiquitin-protein ligase NHLRC1 (EC 6.3.2.-) (Malin) (NHL repeat-containing protein 1)
	UBA52	Ubiquitin-60S ribosomal protein L40 (CEP52)
	RPS27A	Ubiquitin-40S ribosomal protein S27a (Ubiquitin carboxyl extension protein 80)
	UBB	Polyubiquitin-B [Cleaved into: Ubiquitin]
	UBC	Polyubiquitin-C [Cleaved into: Ubiquitin]
CELL ADHESION, EXTRACELLULAR MATRIX	ILK	Integrin-linked protein kinase (EC 2.7.11.1)
	PCDH12	Protocadherin-12 (Vascular cadherin-2)

	LAMP2	Lysosome-associated membrane glycoprotein 2 (LAMP-2)
	MMP2	72 kDa type IV collagenase (EC 3.4.24.24) (72 kDa gelatinase) (Gelatinase A) (Matrix metalloproteinase-2)
	DPYSL3	Dihydropyrimidinase-related protein 3 (DRP-3) (Collapsin response mediator protein 4)
	MAPT	Microtubule-associated protein tau (Neurofibrillary tangle protein) (Paired helical filament-tau) (PHF-tau)
	PCDH12	Protocadherin-12 (Fragment)
	EPM2AIP1	EPM2A-interacting protein 1 (Laforin-interacting protein)
	GFPT1	Glutamine--fructose-6-phosphate aminotransferase [isomerizing] 1 (EC 2.6.1.16)
	GNMT	Glycine N-methyltransferase (EC 2.1.1.20)
	EPM2A	Laforin (EC 3.1.3.-) (EC 3.1.3.16)
	PCYT1A	Choline-phosphate cytidylyltransferase A (EC 2.7.7.15)
	HEL-S-182mP	Glycine N-methyltransferase (EC 2.1.1.20)

TUMORIGENESIS RELATED	MCL1	Induced myeloid leukemia cell differentiation protein Mcl-1 (Bcl-2-like protein 3)
	MUC1	Mucin-1 (MUC-1) (Breast carcinoma-associated antigen DF3)
	SPAG5	Sperm-associated antigen 5 (Astrin) (Deepest) (Mitotic spindle-associated protein p126) (MAP126)

OTHER	VIMP	Selenoprotein S (SelS) (VCP-interacting membrane protein)
	DKFZp686D0638	Putative uncharacterized protein DKFZp686D0638 (Fragment)
	C1QTNF2	Complement C1q tumor necrosis factor-related protein 2
	DCAF7	DDB1- and CUL4-associated factor 7 (WD repeat-containing protein 68) (WD repeat-containing protein An11 homolog)
	DNM1L	Dynamin-1-like protein (EC 3.6.5.5)
	DAB2IP	Disabled homolog 2-interacting protein (DAB2 interaction protein)
	PHLDA2	Pleckstrin homology-like domain family A member 2
	TWIST2	Twist-related protein 2 (Class A basic helix-loop-helix protein 39) (bHLHa39) (Dermis-expressed protein 1) (Dermo-1)
	GRB10	Putative uncharacterized protein GRB10 (Fragment)
	ENPP1	Ectonucleotide pyrophosphatase/phosphodiesterase family member 1 (E-NPP 1)

	SLC17A3	Sodium-dependent phosphate transport protein 4 (Na(+)/PI cotransporter 4)

Figure 1.

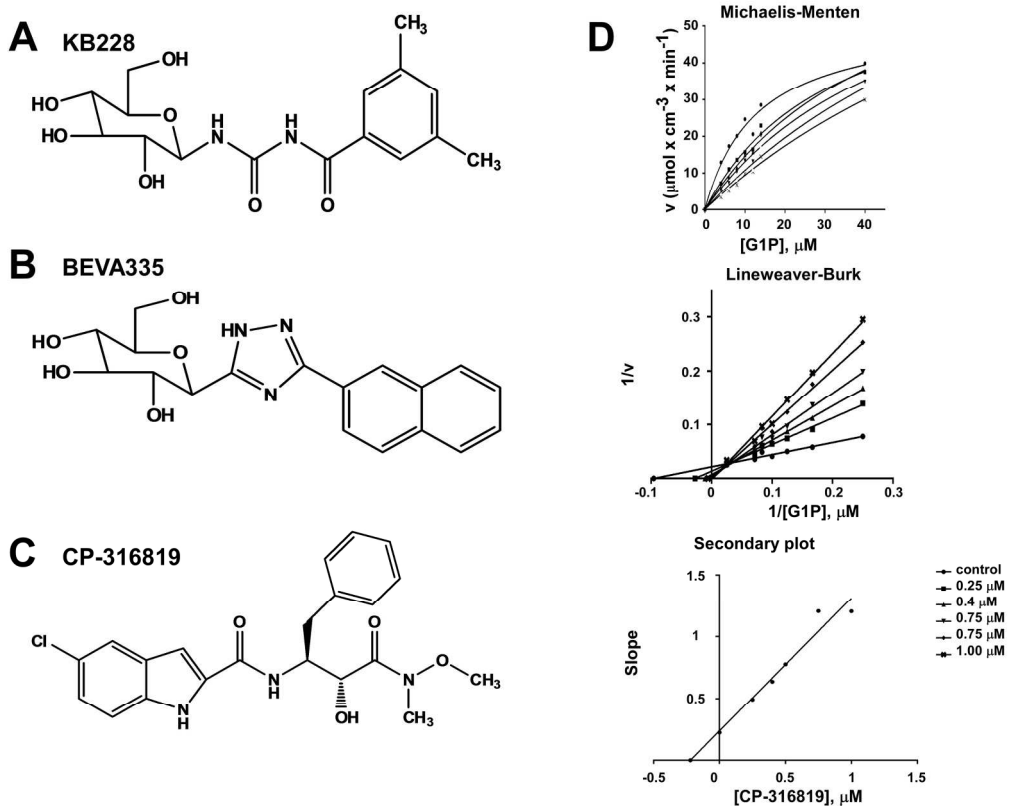

Figure 1. Structures of GP inhibitors
(A) KB228: N-(3,5-dimethyl-benzoyl)-N'-(ß-D-glucopyranosyl)urea, 3 µM final concentration (Ki=937 nM).
(B) BEVA335: 3-ß-D-glucopyranosyl-5-(2-naphthyl)-1,2,4-triazole, 1.5 µM final concentration (Ki=411 nM).
(C) CP-316819: 5-Chloro-N-[(1S, 2R)-2-hydroxy-3-(methoxymethylamino)-3-oxo-1-(phenylmethyl) propyl]-1H-indole-2-carboxamide, 0.5 µM final concentration (Ki=220 nM).
(D) Kinetics inhibition of glycogen phosphorylase b by CP316819 were analysed at constant concentration of glycogen (1 m/V%), and varying concentrations of glucose-1-phosphate (4-40 mM). Replotting the slopes of double reciprocal plots against the effective inhibitor concentrations the secondary plot where analysed, which show the Ki for the inhibitor.

194x179mm (300 x 300 DPI)

Figure 2.

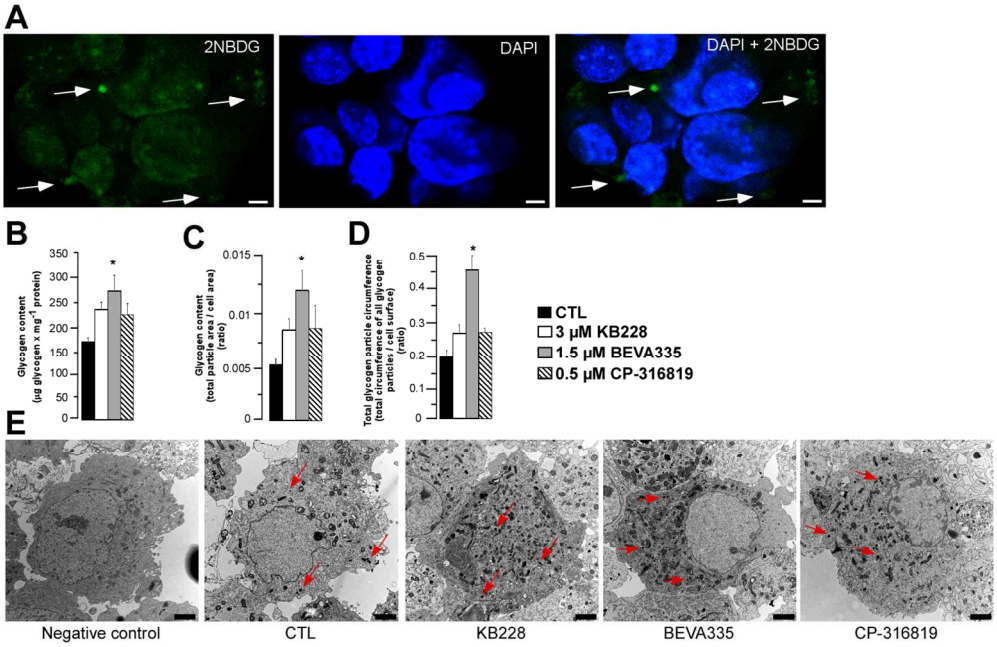

Figure 2. The effects of GPi-s on glycogen content and on the size of glycogen particles in β-cells
(A) In MIN6 cells, the cytosolic localization of glycogen granules was analyzed in confocal microscopy experiments. After incorporation of fluorescent labelled derivative of D-glucose (2NBDG, green) into glycogen the nuclei were visualized by staining with DAPI (in blue). White arrows point to representative glycogen particles. Bars represent 5 µm. Brightness and contrast was adjusted on that panel.
(B) MIN6 cells were treated with GP inhibitors at the concentrations indicated for 24 hours, then glycogen content was determined in phenol-sulfuric colorimetric assays (n=6, in duplicate).
(C-D) Alternatively, glycogen was assessed by morphometric analysis of ultrasections of ferrocyanide-reduced osmium-stained MIN6 cells. (C) Quantification of glycogen content in cells (n=5, 10 cells analyzed per run) and (D) the circumference of the total glycogen particle in cells (n=5, 10 cells analyzed per run) were determined on EM sections.
(E) Representative EM sections are presented. Red arrows point to representative glycogen granules (bars = 2 µm).

259x173mm (150 x 150 DPI)

Figure 3.

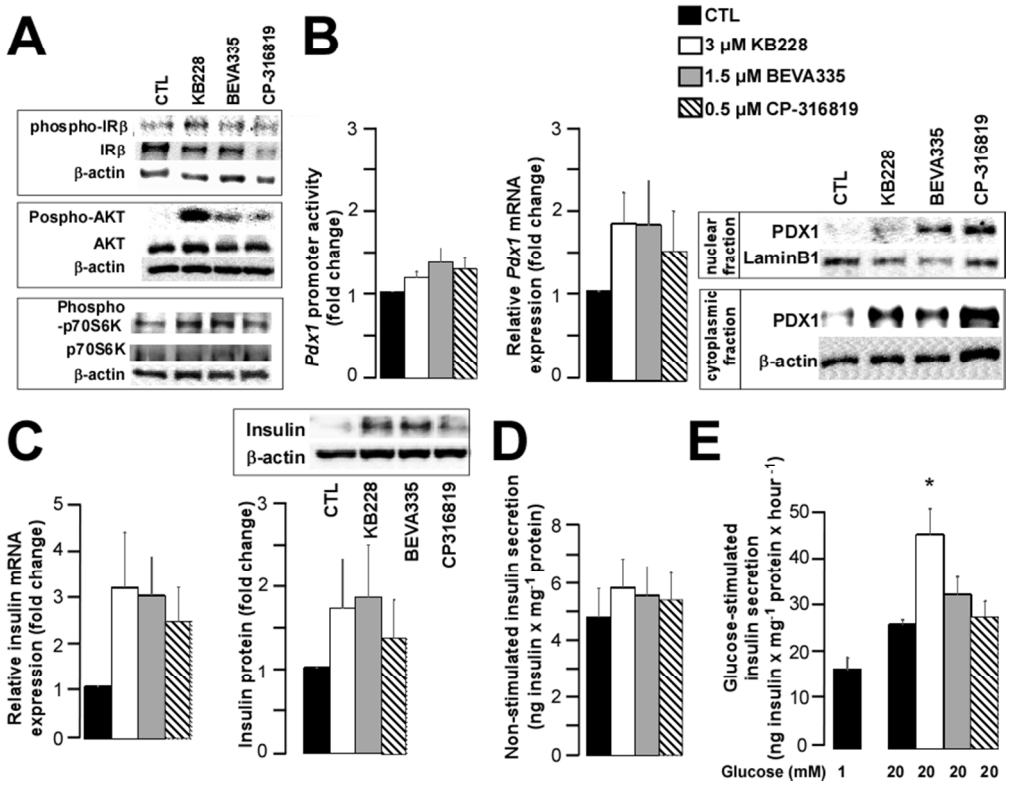

Figure 3. GP inhibitors induce insulin receptor signaling in MIN6 cells
MIN6 cells were treated with GPi-s for 1 day at the indicated concentrations. In these cells (A) phosphorylation of IRβ subunit on Tyrosine 1345, AKT on Serine 473 and S6K on Threonine 389 were assessed by Western blot analysis of phosphorylated and non-phosphorylated forms of the respective proteins. One representative blot is presented. (B) Pdx1 promoter activity (n=5, in duplicate) by luciferase assay and mRNA levels (n=5, in duplicate or triplicate) by RT-qPCR were determined. PDX1 protein levels were determined in the cytoplasmic and nuclear fractions of MIN6 cell lysates by Western blotting. One representative blot is presented here. (C) In GPi-treated cells, insulin mRNA expression (n=5, in duplicate or triplicate), the corresponding protein levels (n=5) as well as (D) insulin release (n=6) were determined. (E) GSIS were analyzed by insulin ELISA Kit (n=5).

154x129mm (150 x 150 DPI)

Figure 4.

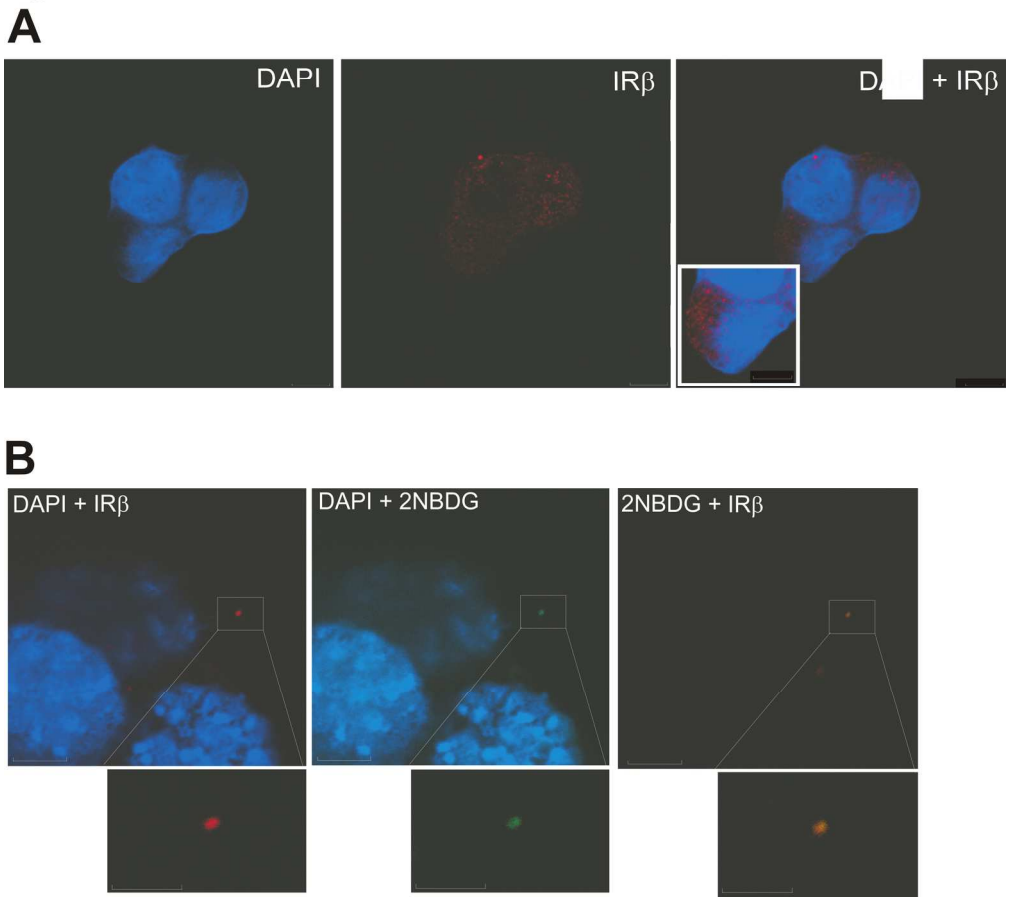

Figure 4. Co-localization of glycogen particles and β subunit of insulin receptor in MIN6 cells.
(A) Localization of IRβ and its (B) co-localization with glycogen in MIN6 cells were assessed in confocal microscopy experiments (n=8). Glycogen was charged with a fluorescent glucose analog (2NBDG, green), IRβ was immunostained using an IRβ-specific antibody and Alexa Fluor 647 secondary antibody (red). Nuclei of the cells were stained using DAPI (blue). Bars represent 5 μm, on the inlay of panel A the bar represents 3.5 μm. IRβ staining was completely lost when the primary antibody was omitted during immunostaining. On the inlay of panel A brightness and contrast was adjusted.

167x153mm (300 x 300 DPI)

Figure 5.

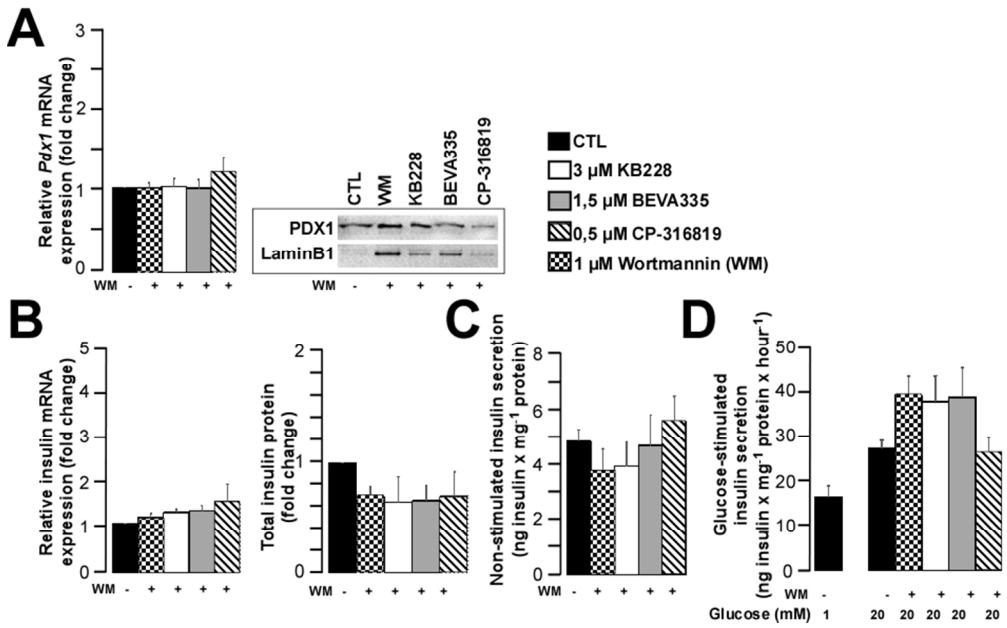

Figure 5. Inhibition of PI3K by WM abolished the effects of GPi-s in MIN6 cells.
MIN6 cells were treated with GPi-s as before and a subset of MIN6 cells were treated with wortmannin (WM, 1 μM, for the last hour of the GPi treatment). In these cells mRNA (n=5, in duplicate) and protein levels (n=5, in duplicate) of (A) PDX1 and (B) insulin were determined. For determination of insulin, total protein was extracted and insulin was quantified by Mouse Insulin ELISA Kit. Finally, (C) non-stimulated, spontaneous (n=5) and (D) glucose-induced (n=5) insulin secretion were assessed.

160x104mm (150 x 150 DPI)

Figure 6.

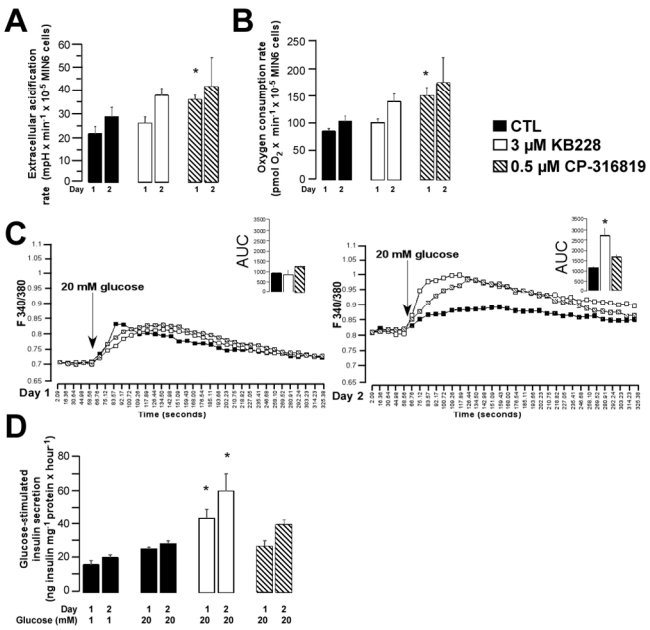

Figure 6. GP inhibitor KB228 and CP-316819 induce the "classical" insulin secretion pathway in MIN6 cells. MIN6 cells were treated with GPi-s for 1 and 2 days. In these cells (A) extracellular acidification rate (ECAR) and (B) cellular oxygen consumption rate (OCR) (n=7, in quadruplicate or octuplicate) were determined by Seahorse extracellular flux analyzer. (C) Calcium influx was induced by 20 mM glucose and was determined by fura-2AM staining (n=5, 6-8 area of interest). Furthermore, GSIS (D) (n=5) was determined by Mouse Insulin ELISA Kit. Insulin baseline was measured at 1 mM glucose concentration, while glucose stimulation was performed with 20 mM glucose similarly to the measurement of Ca2+-oscillation.

263x169mm (150 x 150 DPI)

Figure 7.

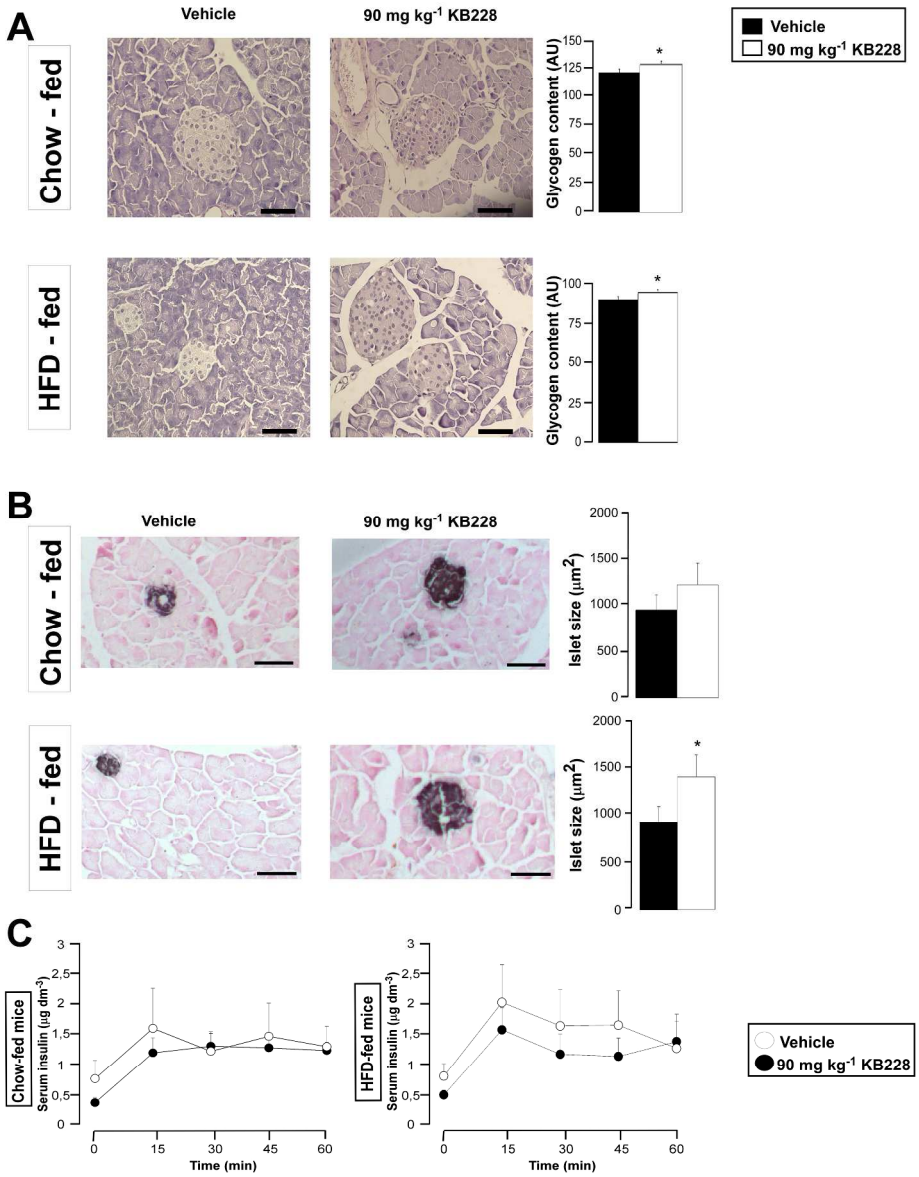

Figure 7. In vivo effects of KB228 treatment
Chow- and HFD-fed C57/Bl6J male mice underwent repeated vehicle or KB228 treatment (weekly, 90 mg kg-1 i.p) for at least three consecutive weeks. After sacrifice (A) glycogen content was evaluated on PAS-stained slides. Representative images are presented (scale bar = 50 µm). PAS positivity was evaluated by measuring the intensity of staining with Image J software. (B) The size of islets of Langerhans were determined on insulin-immunostained histological sections (scale bars = 50 µm). Representative images are shown. Islet size was determined in µm2 by using Image J software. We used Student's t-test (unpaired, two-tailed) for statistical analysis. (C) Glucose-induced increases in serum insulin was determined using insulin-specific ELISA kit.

266x349mm (300 x 300 DPI)